BIOPHYSICS

Human endogenous retrovirus K (HERV-K) envelope structures in pre- and postfusion by cryo-EM

Jeremy Shek[1,2]†, Chen Sun[1]†, Elise M. Wilson[1,2], Fatemeh Moadab[3], Kathryn M. Hastie[1], Roshan R. Rajamanickam[1], Patrick J. Penalosa[1,2], Stephanie S. Harkins[1], Diptiben Parekh[1], Chitra Hariharan[1], Dawid S. Zyla[1], Cassandra Yu[1], Kelly C. L. Shaffer[1,2], Victoria I. Lewis[2], Ruben Diaz Avalos[1], Tomas Mustelin[3], Erica Ollmann Saphire[1,2]*

Human endogenous retroviruses (HERVs) are remnants of ancient infections that comprise ~8% of the human genome. The HERV-K envelope glycoprotein (Env) is aberrantly expressed in cancers, autoimmune disorders, and neurodegenerative diseases, and is targeted by patients' own antibodies. However, a lack of structural information has limited molecular and immunological studies of the roles of HERVs in disease. Here, we present cryo–electron microscopy structures of stabilized HERV-K Env in the prefusion conformation, revealing a distinct fold and architecture compared to HIV and simian immunodeficiency virus. We also generated and characterized a panel of monoclonal antibodies with subunit and conformational specificity, serving as valuable research tools. These antibodies enabled structure determination of the postfusion conformation of HERV-K Env, including its unique "tether" helix, and antibody-bound prefusion Env. Together, these results provide a structural framework that opens the door to mechanistic studies of HERV-K Env and tools for its evaluation as a potential therapeutic target.

INTRODUCTION

Over millions of years, retroviruses have infected germlines of humans and our primate ancestors, integrating into our DNA and passing down through generations. Records of these ancient viral infections are now scattered throughout the human genome, known as human endogenous retroviruses (HERVs). Genomic analyses have revealed that HERV sequences comprise 8% of the human genome, with approximately 98,000 annotated insertions (*1*). HERVs have a canonical retroviral genome like their exogenous counterparts with *gag*, *pol*, and *env* genes flanked by long-terminal repeats containing regulatory elements (*2*, *3*). Over time, most HERV elements accumulated mutations or deletions that rendered them nonfunctional and incapable of producing infectious virions (*3*).

Among these HERVs, the HERV-K (HML-2) family is the most recently acquired insertion; HERV-K insertions have accumulated the least number of deleterious mutations and are thought to be the most transcriptionally active (*4*, *5*). There are ~100 HERV-K full proviral inserts in our genomes, many of which contain complete open reading frames (ORFs) for each of the viral proteins (*6*–*8*). While epigenetic modifications and transcriptional repressors such as CpG methylation, histone acetylation, and chromatin remodeling keep HERV-K transcriptionally silenced in healthy adult cells (*9*, *10*), recent studies reveal that in certain disease states, HERV-K proteins escape suppression and are actively transcribed (*11*–*13*).

Specifically, expression of the HERV-K envelope glycoprotein (Env) protein, encoded by the *env* gene, has been detected in breast, ovarian, prostate, melanoma, leukemia, and other cancers (*14*–*23*). Aberrant Env expression is associated with cancer cell proliferation, tumorigenesis, and disease progression (*24*–*29*). Autoimmune diseases including rheumatoid arthritis (RA), systemic lupus erythematosus (SLE), and type I diabetes (T1D) have also been linked with increased expression of Env (*7*, *30*–*35*). Furthermore, it is evident that the immune system develops an antibody response against Env in many cases and that antibodies against Env may even contribute to the pathogenesis of these malignancies (*7*, *15*, *33*, *36*–*39*). Although much remains to be found about roles of Env in disease, the aberrant expression of Env on the cell surface could be leveraged for immunotherapy and diagnostics. Antibodies targeting HERV-K Env have demonstrated antitumor effects against breast cancer (*40*), engineered chimeric antigen receptor (CAR) T cells targeting Env can inhibit tumor metastasis (*41*, *42*), and mice immunized with a vaccine directed against Env can reject tumors expressing HERV-K Env (*43*). Further, antibodies targeting HERV-K Env neutralize Env-mediated neurotoxicity in the cerebral spinal fluid of patients with amyotrophic lateral sclerosis (ALS) by blocking binding of Env to its receptor (*35*, *39*, *40*). Collectively, these findings suggest Env as a marker or direct therapeutic target in a range of diseases.

Confounding molecular analysis of HERV-K Env function, recognition, and targeting is the lack of any structural information of the HERV-K antigen. While every human bears more than 10 complete copies of HERV-K *env* with the capacity for expression in their genomes, we do not yet know what the protein looks like or how antibodies may target it. In this study, we use stabilizing approaches, antibody discovery, and cryo–electron microscopy (cryo-EM) to reveal structures of the Env ectodomain (Env_{ECTO}) in both the prefusion and postfusion conformations. Our findings report an overall architecture that is distinct from all known retroviral structures. We also illuminate surfaces available for immune recognition and monoclonal antibodies (mAbs) that begin to chart the antigenic landscape of HERV-K Env. The stabilized protein and mAbs open doors for functional studies of Env in disease and structure-based development of new interventions.

[1]Center for Vaccine Innovation, La Jolla Institute for Immunology, La Jolla, CA 92037, USA. [2]Dept. of Medicine, University of California, San Diego, La Jolla, CA 92037, USA. [3]Division of Rheumatology, University of Washington, Seattle, WA 98109, USA.
*Corresponding author. Email: erica@lji.org
†These authors contributed equally to this work.

RESULTS

Stabilization of the HERV-K Env prefusion trimer

There are multiple insertions of the HERV-K in the human genome. Among them, at least 10 loci contain intact ORFs for the *env* gene

(*7*). These HERV-K family *env* genes are classified by the absence (type 1) or presence (type 2) of a 292–base pair (bp) sequence at the 5′ end of the gene, which encodes a signal peptide for plasma membrane surface localization (*44*). Previous studies have generated consensus sequences of the HERV-K proviral genome by comparing HERV-K proviral inserts with the type 2 *env*s. These consensus sequences generate infectious virions (*45*, *46*), are fusogenically active, and have broad tropism (*47*). For this study, we used the unstabilized type 2 Phoenix consensus envelope ectodomain (residues 97 to 632), termed unstabilized HERV-K Phoenix envelope ectodomain (Env_{UNS}), as the starting template for stabilization, given its >97% sequence identity to all HERV-K Envs with expression potential (fig. S1A) (*45*).

HERV-K Env is a class I viral fusion protein comprising an expected receptor-binding/surface protein subunit (SU) and a fusion/transmembrane protein subunit (TM). Three noncovalently bound SU-plus-TM protomers trimerize on the cell surface (*48*). Consistent with the metastability of class I viral fusion proteins, unstabilized Env can spontaneously adopt the more energetically stable postfusion conformation, in which the SU subunits disassociate, leaving the TM subunits to fold into a six-helix bundle (6HB) (*49*, *50*). This metastability poses a major obstacle to the expression and stability of prefusion conformation Env protein that would be amenable to structure determination by cryo-EM.

To overcome the problems associated with viral glycoprotein metastability, we explored methods that have been previously successful in the engineering of other viral envelope glycoproteins, introducing functional mutations to confer stability to the prefusion conformation. Modifications we designed include (i) helix-breaking proline mutations, (ii) intersubunit disulfide linkages, and (iii) additional multimerization domains (*51*–*53*). We screened and tested mutants for expression, posttranslational processing, and oligomerization, using an iterative process of AlphaFold- and DeepCoil-driven predictions (*54*, *55*) to determine where to place helix-breaking mutations to break the long heptad repeat 1 (HR1) helix that would otherwise drive formation of the postfusion HB. Twenty-two mutants with one or two prolines within the HR1 sequence were evaluated for expression and oligomerization. The best-behaved sequences were then input into AlphaFold to generate new model predictions that were more "prefusion-like." From these models, we next designed 13 potential cysteine pairs using structural visualization in ChimeraX (*56*) and the Disulfide by Design 2.0 server (*57*) to form disulfide bonds between SU and transmembrane protein ectodomain (TM_{ECTO}). In parallel, we assessed the utility of heterologous oligomerization domains, modified linker lengths, and evaluated expression and posttranslational processing in different eukaryotic cell lines by size exclusion chromatography (SEC) and SDS–polyacrylamide gel electrophoresis (SDS-PAGE).

Among the hundreds of mutations and modifications we screened, the combination of one introduced cysteine pair between SU (V437C) and TM_{ECTO} (V498C), two point mutations that altered the furin cleavage motif from RSKR to RRRR, and addition of the T4 fibritin trimerization domain at the C terminus of TM_{ECTO} together resulted in the expression of stabilized, prefusion Env_{ECTO} trimers (Fig. 1, A and B, and fig. S2). SEC and SDS-PAGE analyses of Env_{ECTO} expressed in *Drosophila* S2 insect cells indicate that Env_{ECTO} is efficiently processed by furin into SU and TM_{ECTO} subunits, which are joined by a disulfide bond, and that this Env oligomerizes as a stable trimer in solution (fig. S2, B to E). We evaluated the Env_{ECTO} constructs using nano differential scanning fluorimetry and observed an increase in thermal stability, with melting temperatures (T_m) rising from 46.0° ± 0.2°C in the unstabilized Env_{UNS} to 53.8° ± 0.1°C in the stabilized Env_{ECTO} (fig. S2, F to H). In addition, the stabilized Env_{ECTO} remained stable from pH 7.5 down to 5.0, with only a minor T_m reduction to 52.9° ± 0.1°C in acidic conditions, which are required for Env-mediated fusion (fig. S2I) (*58*).

Purified Env_{ECTO} trimers were applied to graphene oxide–coated grids and vitrified for cryo-EM. A total of 81,000 particles from 8603 movies were processed with CryoSPARC (*59*) to obtain a reconstruction at a 2.2-Å global resolution (Fig. 1C and fig. S11).

The architecture of the prefusion HERV-K Env trimer

With the high-resolution map we obtained, we were able to build nearly the entirety of Env_{ECTO} in the prefusion conformation with only residues at the N- and C-terminal ends of SU (97 to 99 and 460 to 465) and the N-terminal, membrane-proximal end of TM_{ECTO} (621 to 632) unmodeled (Fig. 1, C and D). Overall, the soluble HERV-K Env_{ECTO} prefusion trimer adopts an elongated shape akin to an inverted tripod with a height of ~117 Å along the vertical axis and a width of ~83 Å. In the trimer, the SU subunits sit above their TM counterparts and are shaped like prongs that extend 49 Å from the highest point of the TM_{ECTO} near the trimer axis (Fig. 1D). At the trimer apex, between the assembled three SUs, is an open central cavity with a solvent-accessible surface area of approximately 7000 Å. Although the furin cleavage motif (residues 461 to 465) is unmodeled, the C terminus of SU ending just before the furin motif at residue 459 folds as a downward-pointing α helix (α4) toward the membrane surface and forms a bundle with the C-terminal helices (α12) of the TM_{ECTO} (Fig. 1, D and E). The distance between the two residues flanking the furin sequence (V459 on SU and F466 on TM) is 53 Å. If uncleaved, this seven–amino acid span could reach ~25 Å. A separation of 53 Å indicates that upon cleavage, the newly formed termini must displace from each other, with the SU C terminus moving toward the foot of the trimer while the TM_{ECTO} N terminus burying itself toward the central coiled coils. This ~30-Å displacement explains why attempts to engineer an uncleavable Env_{ECTO} did not result in successful expression or trimerization and instead resulted in misfolded proteins with improper quaternary structure.

The structure of env SU

The SU subunit (residues 97 to 465) is a 369–amino acid polypeptide comprising 4 α helices and 25 β strands. SU consists of two main subdomains, here termed the core and the base (Fig. 1E).

The core domain, formed by residues 172 to 378, is membrane-distal at the trimer apex. It features a β sandwich fold in which one face, comprised of five antiparallel strands (β6, β7, β14, β17, and β18), forms an elongated, distorted sheet, while the opposing face is formed by two short antiparallel strands (β13 and β15). Two disulfide bridges stabilize flexible loops in the core structure (table S2). The first, C275-C282, stabilizes a surface-exposed loop at the apex of SU. The second disulfide, C227-C246, anchors the loop flanked by the two cysteine residues, the largest and most flexible loop in our model. At higher map thresholds (e.g., 11σ), the volume for the residues 233 to 239 of this loop are unresolvable. Applying a blur factor of +50 $Å^2$ revealed continuous density, which allowed us to trace and model the loop in its entirety.

The SU base domain, formed by residues 97 to 171 plus 379 to 439, is the more membrane-proximal of the core-base pair and is responsible for mediating interactions with the TM subunit in the prefusion conformation. The base consists of a distorted β barrel

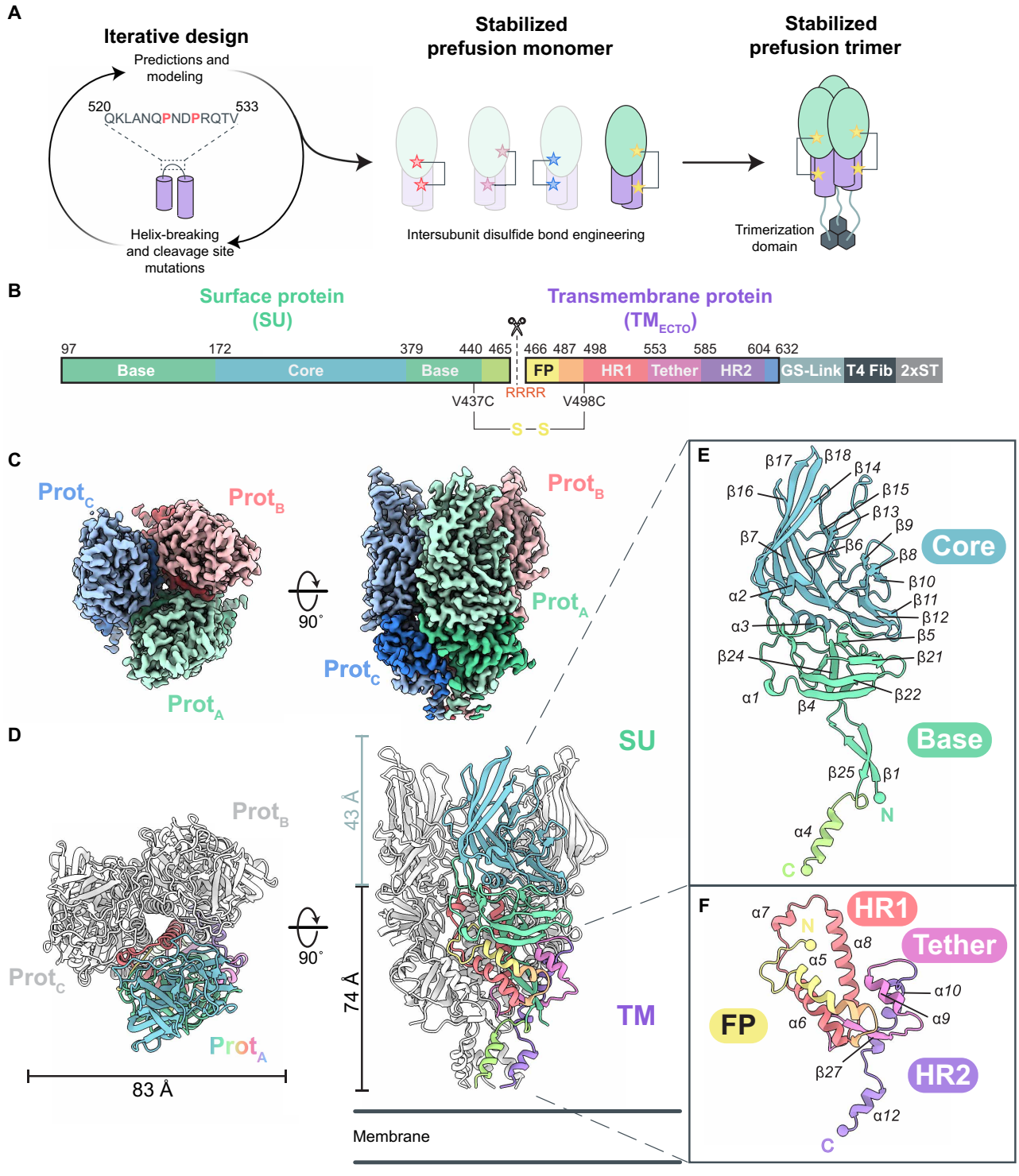

Fig. 1. Stabilized prefusion HERV-K Env enables high-resolution structure determination by cryo-EM trimer. (**A**) Protein engineering workflow for stabilization of the prefusion HERV-K Env$_{ECTO}$. (**B**) Primary structure annotation of Env$_{ECTO}$ construct. Domains are color-coded. Abbreviations: FP, fusion peptide; HR1, heptad repeat 1; HR2, heptad repeat 2; GS-Link, 12-amino acid GGS linker; T4-Fib, T4 fibritin foldon trimerization domain; 2xST, Twin Strep-Tag II. Regions boxed in black are sequences of Env$_{ECTO}$. Black scissors indicate the furin cleavage site that cleaves Env into its SU and TM subunits. Engineered disulfide bond mutations and furin-cleavage motif modifications are annotated. (**C**) 2.2-Å resolution cryo-EM map of the HERV-K Env$_{ECTO}$ trimer (colored using green, red, and blue shades) (**D**) Cartoon representation of the HERV-K Env$_{ECTO}$ trimer. Protomer A is colored in a rainbow as described in (B). The remaining two protomers are colored in white. (**E**) Isolated cartoon representation of the SU subunit from an individual protomer. (**F**) Cartoon representation of the TM$_{ECTO}$. Both (E) and (F) are colored using the same color scheme as (B) and (D). N- and C-terminal Cα atoms for each subunit are represented as spheres.

structure (β2, β4, β5, β20, β21, β22, and β24) positioned above the β1-β25 sheet where the N and C termini join. This β sheet extends downward toward the membrane. The C-terminal end of the SU subunit is proximal to the very bottom of the ectodomain, where α4 is located, directly preceding the furin cleavage motif (residues 461 to 465), which is not resolved. The SU subunit does not form any contacts with neighboring SUs in the trimer in our static structure and does not appear to contribute to trimeric interactions.

The structure of prefusion TM

The TM subunit is responsible for the membrane fusion mechanism of retroviral Env. The prefusion TM ectodomain structure presented here comprises eight α helices and two β strands (Fig. 1F). Consistent with class I viral fusion proteins, TM_{ECTO} contains a hydrophobic fusion peptide followed by HR sequence motifs, HR1 and HR2. The fusion peptide (residues 466 to 486) begins as an unstructured coil that transitions into α5, sitting above α6 of HR1. The first HR motif, HR1 (498 to 552), is divided into three α helices: α6, α7, and α8. The third, α8, is amphipathic. The hydrophobic side of the α8 helix faces the center of the trimer axis and forms the central coil. HR1 and HR2 are linked by a 32-residue tether region that contains a CX_7C disulfide motif (C551-C559) specific to betaretroviral envelope proteins (*48*). HR2 (residues 585 to 603) extends proximally toward the membrane, with the C terminus of TM_{ECTO} forming a bundle at the bottom of the trimer (Fig. 1, D and F).

Prefusion TM clamps the SU base domain with a C-shaped clasp

Within each protomer, SU contacts its TM partner via the seven-stranded β barrel and the terminal β1-β25 sheet of the base domain. The prefusion TM_{ECTO} encircles the extended N- and C-terminal strands of the base, forming a C-shaped clasp (Fig. 2, B and C). Helices α6 and α7 partially envelop the extended N- and C-terminal strands of SU before reversing direction and extending behind where β27 hydrogen bonds to β25, joining the β1-β25 sheet in an antiparallel fashion (Fig. 2D). The TM completes its wrapping around SU with α9 enclosing the remaining portion of the clamp. Side-chain nitrogen atoms from R576 and W572 form a hydrogen bond network with the backbone oxygen of H492 and S493, effectively closing and locking the clasp (Fig. 2B). As a result, the HERV-K TM forms a near-complete ring underneath the SU base around the terminal β sheet (Fig. 2C).

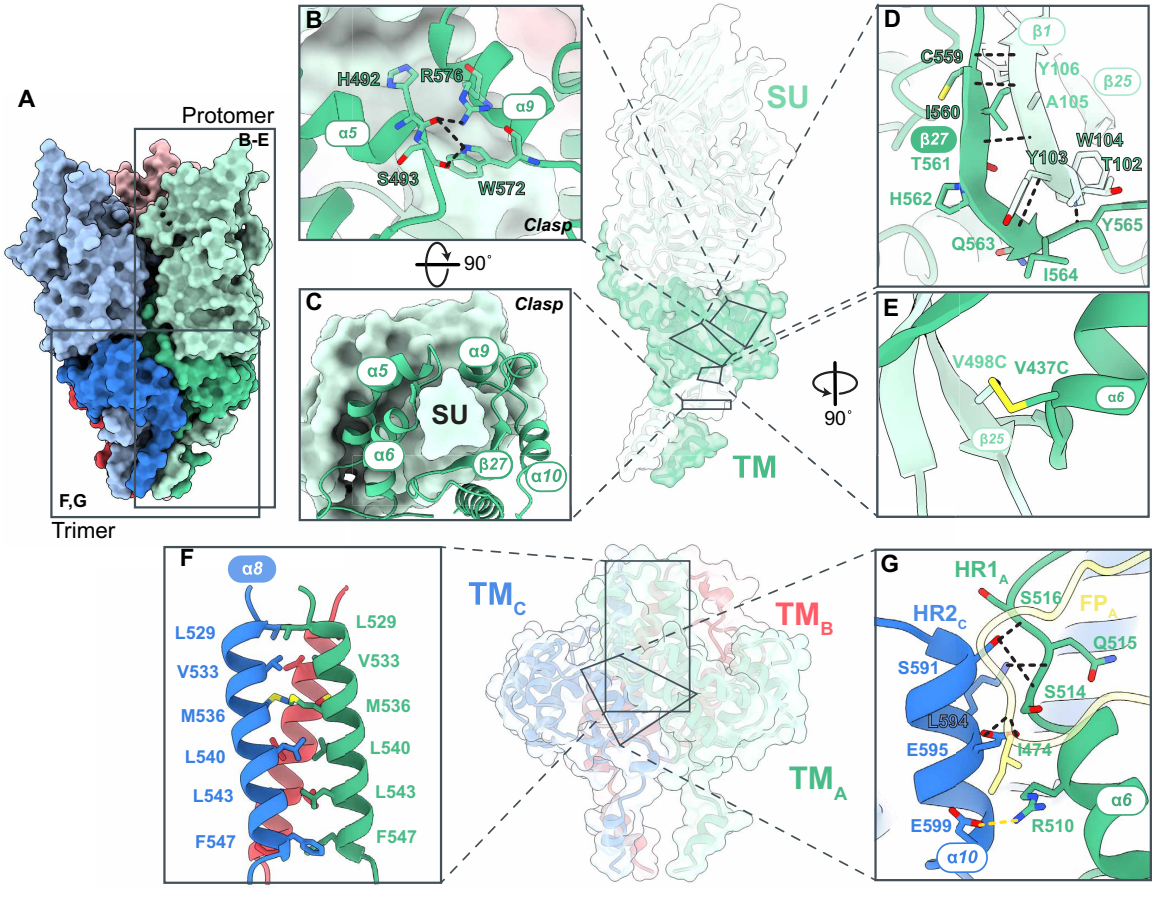

Fig. 2. Protomer and trimer interfaces of prefusion Env. (**A**) The prefusion Env_{ECTO} trimer displayed using a molecular surface representation. SU + TM protomer interactions are shown in (**B** to **E**) and trimeric interactions are shown in (**F**) and (**G**). (B) The clasp formed by the TM around the base domain of the SU viewed from the front. Residues involved in clasp locking are shown as sticks. (C) The C-shaped clasp formed by TM around SU viewed from bottom-up. [(B) and (C)] SU is shown as a light green surface and TM is a dark green cartoon. (D) β Sheet formation between the β1 strand from SU (light green) and the β27 strand from TM (dark green). (E) The engineered disulfide bond between the SU and TM to stabilize Env_{ECTO}. (F) Side view of the central coiled coil. Hydrophobic residues facing the interface from each helix are shown as sticks. (G) The interactions between adjacent prefusion TM subunits distal from the central coils. The fusion peptide of TM_A is colored in yellow. [(B), (D), and (G)]. Hydrogen bond interactions are shown by dashed black lines, and salt bridges are shown in dashed yellow lines.

Dissociation of the receptor-binding subunit from the fusion protein subunit is a trigger of conformational change to the postfusion state (*49*, *50*). To prevent the dissociation of the noncovalently bound SU and TM subunits, part of our previously described engineering was the introduction of an intersubunit disulfide between residues 437 on SU and 498 on TM (Fig. 2E). The engineered disulfide anchors the N terminus of the TM between the fusion peptide and HR1 at the membrane-proximal end of strand β25, to the base of SU. This disulfide stabilizes the prefusion conformation of Env by preventing the HR1 refolding and extension that would be needed for transition to the postfusion conformation (fig. S6B).

Trimerization is driven by TM-TM interactions

Much like other class I viral fusion proteins such as the HIV Env, Ebola GP, RSV F, and influenza hemagglutinin (HA) proteins, the Env trimer is stabilized by the presence of a central coiled coil (*49*, *60*–*63*). In HERV-K Env, the coiled coil is formed by helix α8 (residues 529 to 548) in the HR1 sequence of each TM subunit, via hydrophobic interactions between the a and d positions of the HRs at the central axis (Fig. 2F). We found that both the length of the α8 helix as well as the absence of helix-breaking mutations are crucial for Env trimerization. We initially followed the HIV-1 SOSIP strategy (*64*) of inserting kinks within the junction between α7 and α8 of Env, mutating residues to prolines, and did notice an increase in expression with three such mutants. However, our best-expressing mutant, L529P, yielded primarily Env monomers (fig. S3). We hypothesize that the proline insertion destabilizes the secondary structure of the N terminus of α8, decreasing the number of hydrophobic interactions in the central coiled coil (Fig. 2F), and thereby weakening the trimer complex. Trimerization of Env_{ECTO} was achieved by reverting P529 back to its native lysine.

In the HERV-K Env trimer, the TM-TM interaction is further reinforced by hydrogen bonds and salt bridges interfacing HR2 α10 with the adjacent TM fusion peptide and HR1 α6 (Fig. 2G). This network ensures that the outer edges of the prefusion TMs are fastened together in the trimeric complex.

Env is moderately glycosylated

The HERV-K Env_{ECTO} sequence contains 10 possible N-glycosylation sites on each monomer, 6 on the SU subunit, and 4 on the TM subunit (table S3). All 10 potential glycosylation sites are occupied, and we were able to build the *N*-acetylglucosamine cores for all the glycans (fig. S4A). For the glycan at N128, we could also model a mannose residue on each branch (fig. S4B). For the N566 glycan, we observe strong density corresponding to an α1-6 linked fucose (fig. S4C), which we modeled. Using the GlycoSHIELD pipeline (*65*), we modeled all glycosylation sites except for N566 as mannose-5. For N566, we used a mannose-5 with an α1-6 linked fucose. Solvent-accessible surface area analysis of the glycosylated protein using a probe radius of 1.4 Å indicates that 31% of the surface of SU is shielded compared to the unglycosylated protein, with the apex particularly solvent exposed. The TM is more shielded with 57% of its surface covered by glycans (fig. S4, D and E). Together, the cryo-EM data indicate that HERV-K Env_{ECTO} has a 1:53 ratio of glycans to amino acids and is less shielded than the envelope ectodomains of HIV-1 (1:23) and simian immunodeficiency virus (SIV) (1:27), but comparable to exogenous retroviral Envs such as Jaagskiete sheep retrovirus (1:49) or endogenous Envs such as Syncytin-1 from HERV-W (1:60) and Syncytin-2 from HERV-FRD (1:50) (*66*–*68*). These findings indicate that HERV-K Env bears a moderate glycan shield, consistent with levels observed in other retroviruses, without the extensive shielding characteristic of lentiviral envelopes.

HERV-K Env adopts a fold distinct from that of other retroviral envelopes

This structure of the Env is the first prefusion trimer complex structure of any HERV. The only other full endogenous retroviral Env structure yet available is from a hookworm endogenous viral element, a type II structure similar to flavivirus envelope proteins (*69*). Further, the HERV-K envelope structure is also the only prefusion structure available for any betaretrovirus, whether endogenous or exogenous. Among all human retroviruses, prefusion Env trimer structures are only thus far solved for the lentiviruses HIV-1 and SIV (*60*, *70*). For HERV-K Env, the only similarities in overall architecture with HIV-1 and SIV Env are that they are gathered into trimers, SU is membrane distal, while TM is membrane proximal and aspects of TM topology. For example, in all three retroviral trimers, SU (or gp120) are held in the prefusion trimer by TM (or gp41) using a clasp or collar structure formed by the α helices from the HR1 and HR2 domains (Fig. 2, B and C). Overall, however, the global shape, secondary structural elements, and folds differ extensively between HERV-K Env and the HIV-1/SIV lentiviruses.

Comparison of the HIV-1 and SIV envelope trimer ectodomains thus far resolved to this structure of the HERV-K Env_{ECTO} reveals that HERV-K Env adopts a more streamlined form, primarily shaped by the SU protein. Compared to Env, the HIV and SIV trimers are shorter and wider, with heights ranging from 95 to 103 Å and widths between 108 to 120 Å (Fig. 3A) and 117 Å tall and 83 Å wide for HERV-K Env.

The envelope glycoprotein of HIV-1 is highly dynamic, spontaneously transitioning between multiple conformational states that influence binding of antibodies, CD4, and coreceptors (*71*). Compared to each of the three described HIV-1 Env conformations, our structure of HERV-K Env_{ECTO} is, in general, more like the closed, unliganded conformation of HIV-1 gp140 (PDB:5CEZ), but the global root mean square deviation (RMSD) is very high at 23 Å (Fig. 3A). The occluded conformation of HIV-1 (PDB:7TFO), triggered by CD4 binding, differs from HERV-K Env by an RMSD of 27 Å, and the fully open (PDB:5VN3), CD4-bound, V3 loop exposed conformation differs by an RMSD of 38 Å. For HIV-1, conformational dynamics are required for receptor and coreceptor binding. In contrast, in HERV-K Env, the presumed receptor binding site is exposed at the trimer apex.

The individual SU protein of HERV-K Env has a previously unseen fold, as revealed by a systematic structural fold search using Foldseek, DALI, and HHpred servers (*72*–*74*). The global RMSDs for HERV-K SU with any of HIV-1 gp120, SIV gp120, or Syncytin-2 SU are each >23 Å, and no other protein in the databases aligns at all with HERV-K SU (Fig. 3B). The area of greatest structural homology is the base domain of HERV-K, a region that is functionally analogous to the inner domain of HIV-1/SIV gp120. Both the HERV-K base domain and the HIV/SIV inner domain contain a distorted β barrel and a membrane-proximal β sheet (Fig. 3B), and both are responsible for TM/gp41 interactions. Outside the base/inner domain, the SU structures are quite different. HERV-K SU is vertically elongated and is composed primarily of β strands, with a discernable, five-stranded β sheet in the core. In contrast, HIV-1 and SIV gp120s are a mixture of β sheets and α helices. Further, the lentiviral gp120s are larger than HERV-K SU (~470 to 510 versus 369 amino

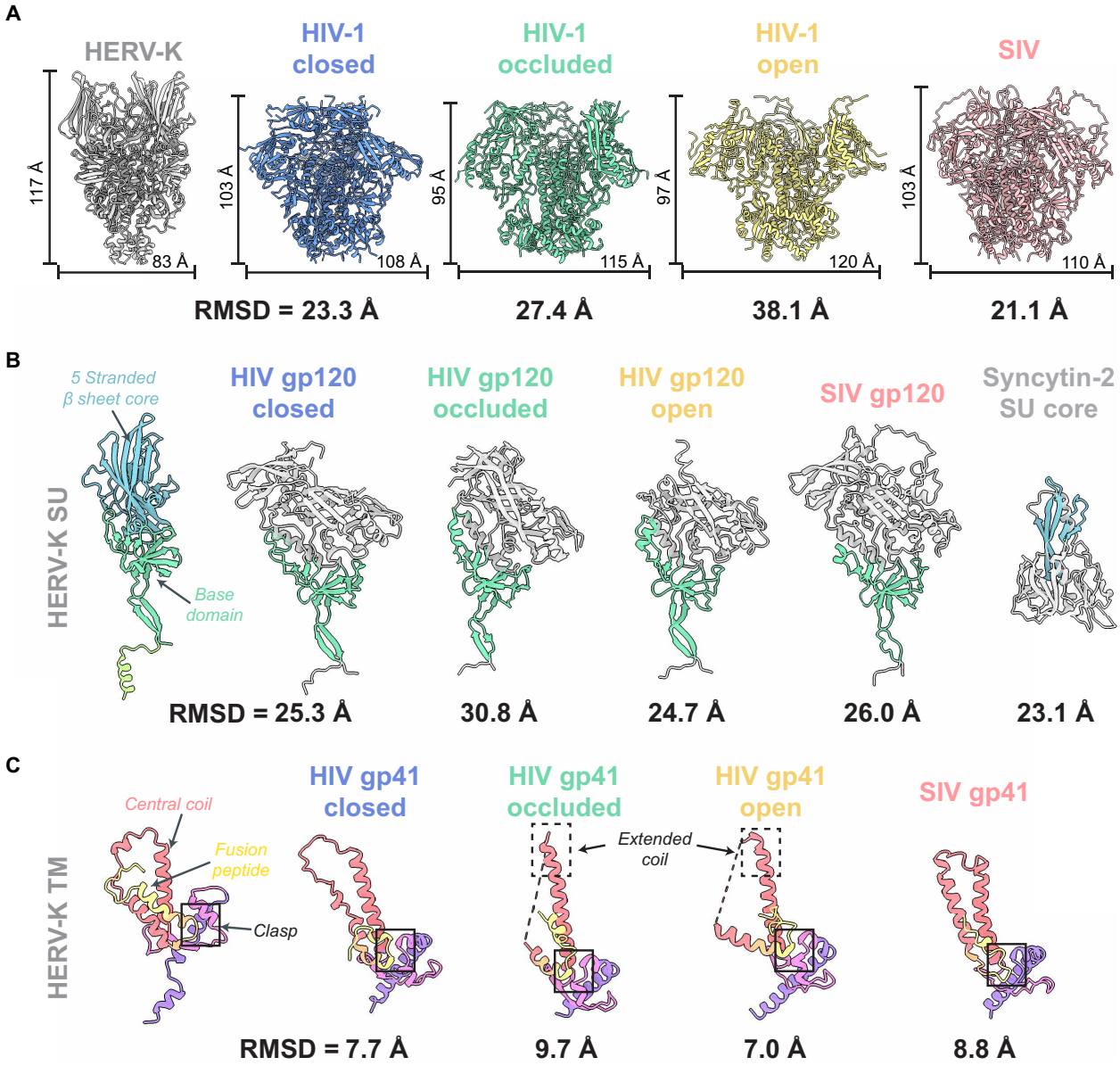

Fig. 3. Prefusion HERV-K Env has a unique fold compared to previously solved prefusion retroviral structures. (**A**) Models of HERV-K Env, HIV Env (closed (PDB:5CEZ), occluded (PDB:7TFO), open (PDB:5VN3), and SIV Env (PDB:7T4G) ectodomain trimers. Approximate heights and widths of each complex were measured using ChimeraX (*56*). (**B**) Comparison of receptor-binding subunits (SU: HERV-K, Syncytin-2; gp120: HIV, SIV). HERV-K Env SU is colored by subdomain, while the other receptor binding subunits are colored in light gray. Shared structural features to HERV-K SU are colored and labeled with their respective colors. (**C**) Comparison of fusion protein subunits (TM: HERV-K; gp41: HIV, SIV) in prefusion conformation. HERV-K Env TM is colored by subdomain. Similar structural features presented on the HIV and SIV gp41 subunits are colored similarly to TM. The C-shaped clasp that encloses the SU/gp120 base domain is boxed in black on each TM/gp41. The HR1 central coil in the occluded and closed conformations of gp41 are extended at the N-terminal ends of the helix, highlighted by the dashed box. Calculated all-atom RMSD values against the HERV-K Env complex or respective subunit are displayed under each structure.

acids), and bear both an outer domain and V1V2 variable regions, which are critical for immune evasion. In contrast, HERV-K SU forms a single-domain structure, and its sequence across endogenous loci is highly conserved, reflecting likely derivation from a common ancestral source and the absence of immune-driven selective pressure (fig. S1). Conservation of HERV-K Envs is an advantage for the development of diagnostics and immunotherapeutics.

The human Syncytin-2 protein is critical for syncytiotrophoblast formation during placental development and is a co-opted envelope protein from the gammaretroviral HERV-FRD, inserted into the genome over 40 million years ago (*75*). Although the core domain of the Syncytin-2 SU subunit has been solved (PDB:7OIX), its full SU has not yet been resolved, either alone or in a trimeric complex with its TM (*76*). The Syncytin-2 SU core does, however, appear to share the β sheet formed by five antiparallel β strands extending upward (Fig. 3B). In Syncytin-2, the short loops that connect the antiparallel strands of this sheet form the binding site for MFSD2A, a membrane-embedded lysophosphatidylcholine lipid symporter (*76*), but it is

not yet known whether the equivalent loops in HERV-K Env play a role in receptor or cofactor binding.

While the HERV-K SU subunit is distinct from the lentiviruses, the TM_{ECTO} subunit in its prefusion conformation exhibits a fold that is more structurally similar to that of prefusion HIV-1 and SIV gp41/TM, with global RMSDs ranging from 7 to 10 Å (Fig. 3C). The TM/g41 of all three viral envelopes share similar tertiary structures, starting with the N-terminal fusion peptide continuing through the C-shaped clasp predominantly composed of α helices that wrap around the SU/gp120 terminal β sheets. A long, vertically aligned α helix, which in HERV-K TM is α8 in the HR1 domain, is also present in HIV-1 and SIV gp41/TM, and in each trimer, forms the central coiled coil crucial for envelope trimerization (Fig. 3C). This central coil structural feature is common among class I fusion proteins, even beyond retroviruses (*50*).

Anti–HERV-K Env mAbs targeting both subunits and distinct conformations of Env

Given the metastability of viral glycoproteins, both prefusion and postfusion conformations of HERV-K Env are likely present on cells expressing Env. Thus, we sought to also solve the structure of the HERV-K TM ectodomain in its postfusion conformation. However, at ~38 kDa, the postfusion TM_{ECTO} trimer is below the optimal size for single-particle cryo-EM reconstruction, and attempts to solve the structure of TM_{ECTO} in isolation were hampered by poor contrast as well as aggregation. To overcome these limitations, we sought mAbs that could bind specifically to folded Env conformations and facilitate structure determination.

Commercially available mAbs HERM-1811-5 and HERM-1821-5 (Austral Biologicals) were elicited by immunization with *Escherichia coli*–produced glycoproteins. They recognize linear epitopes and therefore cannot discern properly folded from misfolded protein and were not suitable for structural studies of Env (Fig. 4).

To address this gap, we immunized BALB/c mice with recombinant, unstabilized Env_{UNS} produced in *Drosophila* S2 insect cells. Using a Bruker Beacon, followed by biochemical characterization, we selected a subset of nine mAbs from the panel that would together broadly cover the range of conformational (pre and postfusion) and subunit (SU and TM) specificities (Fig. 4A). We screened antibodies on enzyme-linked immunosorbent assay (ELISA) coated with either purified Env_{UNS}, which contains both SU and TM_{ECTO} in a mixture of pre and postfusion conformations, or with postfusion TM_{ECTO} alone. Five of the mAbs are bound to both Env_{UNS} and postfusion TM_{ECTO}, while the remaining four bound strongly only to Env_{UNS} (Fig. 4A). To determine whether these mAbs recognize linear or conformational epitopes, we denatured Env_{UNS} or postfusion TM_{ECTO} at 95°C with dithiothreitol (DTT) for 10 min and screened the mAbs using ELISA again. Seven mAbs bound to either denatured Env_{UNS} or postfusion TM_{ECTO}, revealing that they likely bind to linearized epitopes. Kenv-6 only binds Env_{UNS}, and fails to bind denatured or postfusion TM_{ECTO}, indicating that it recognizes a conformational epitope on SU. In contrast, Kenv-4 showed preferential binding to postfusion TM_{ECTO} compared to Env_{UNS}, and, while it retained some reactivity with denatured TM_{ECTO} (Fig. 4A), later structural analyses confirmed recognition of a postfusion epitope. Western blot analysis using Env_{UNS} was performed with each mAb to further confirm subunit and conformational specificities (Fig. 4B), with only Kenv-6 and Kenv-4 not binding to fully linearized and denatured Env.

Together, we found that three mAbs are SU specific (Kenv-6, Kenv-10, and Kenv-14) and six are TM specific (Kenv-1, Kenv-2, Kenv-3, Kenv-4, Kenv-7, and Kenv-8). Two antibodies, Kenv-6 and Kenv-4, bind to conformational epitopes on folded SU and postfusion TM, respectively (Fig. 4C). The conformational antibodies prove especially valuable. Kenv-4 could now be used to facilitate structural determination of the postfusion TM_{ECTO}, while Kenv-6 would serve as a key tool for detecting properly folded SU in both biochemical assays and biological samples.

We sought to further validate antibody recognition to see whether these mAbs would recognize HERV-K Env expressed in human patient samples beyond recombinant protein. We found that five of these antibodies, Kenv-1, Kenv-2, Kenv-3, Kenv-6, and Kenv-7, are able to stain isolated neutrophils from both patients with SLE and RA (Fig. 4D), which have been previously reported to express Envs from two HERV-K loci: HERV-K102 (1q22) and -K108 (7p22.1) (*7*, *32*, *33*, *37*). We observed primarily internal staining of the neutrophils, consistent with expression mostly from the K102 locus (*32*). K102 encodes for a type 1 Env lacking a canonical signal peptide and impairs trafficking to the plasma membrane. In contrast, these mAbs did not have any level of detectable antibody binding to neutrophils from healthy donors, confirming their specificity.

Cryo-EM structure of the postfusion HERV-K Env TM

To resolve the structure of the postfusion conformation of Env, we expressed TM_{ECTO} (residues 498 to 603) fused to an N-terminal maltose-binding protein (MBP) tag via a GS linker and a human rhinovirus (HRV) 3C protease cleavage site, followed by a T4 fibritin trimerization domain (Fig. 5A). Residues 466 to 497 and 604 to 632 were not expressed because of hydrophobicity of the fusion peptide or predicted flexibility. The purified TM_{ECTO} fusion protein was first complexed with Fab fragments of the Kenv-4 mAb and then treated with 3C protease to remove the MBP, which prevented aggregation of TM_{ECTO} alone (Fig. 5A and fig. S5). The TM–Kenv-4 complex was purified by SEC, and 696,758 particles from 19,225 movies yielded a 2.8-Å reconstruction by cryo-EM (Fig. 5B and fig. S13). With the final map, we were able to model residues 502 to 548 and 567 to 603 (Fig. 5C).

The HERV-K TM ectodomain in the postfusion conformation consists of HR1, an internal "tether" region (includes the $^{551}CX_7C^{559}$ motif), and HR2 (Fig. 5, A and D). These three features assemble into a 6HB, a structural hallmark of the postfusion conformation in type I viral glycoproteins (Fig. 5, C and D). At the center of the 6HB, the HR1 helices form the central trimeric coiled coil, while the HR2 and tether helices adopt an antiparallel orientation, packing against the outer surface of the HR1 (Fig. 5C).

The HR1 helix features the repeating seven–amino acid sequence pattern with hydrophobic residues occupying the a and d positions, facilitating interhelical, hydrophobic packing interactions within the trimer (fig. S6). A four-residue stutter ($^{522}LANQ^{525}$) disrupts the regular heptad pattern in the HR1 region (Fig. 5D), a feature missing from the HIV-1 and SIV lentivirus gp41, but observed in influenza HA, Ebola virus GP, lymphocytic choriomeningitis virus GP, and endogenous retroviral envelopes: Syncytin-1 and Syncytin-2 (*77*–*80*). This stutter causes deviations from the ideal helix packing geometry, leading to localized unwinding of the coiled coil. This has been thought to impart flexibility to the helices and the trimeric core (*77*, *81*).

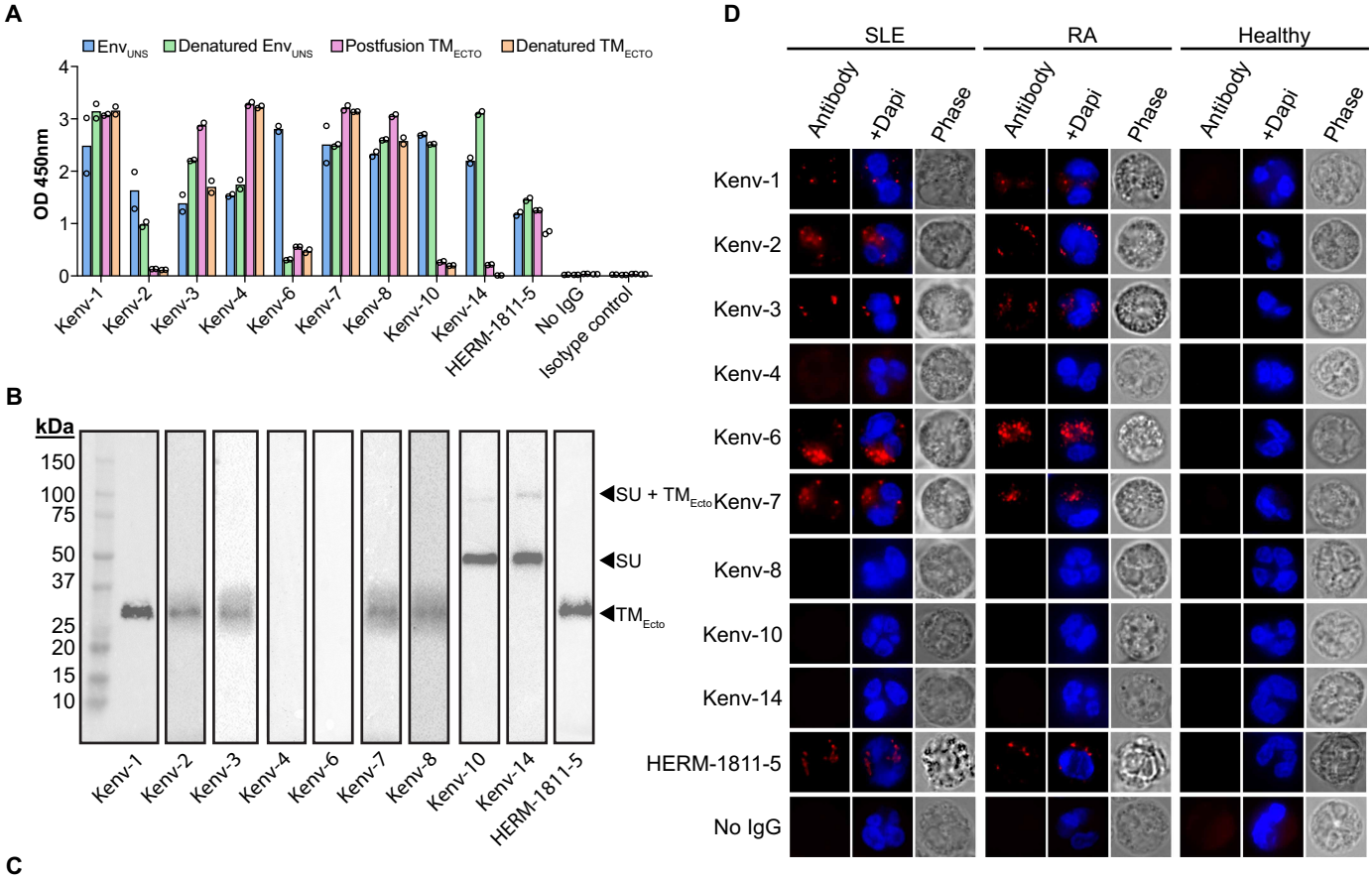

C

Antibody name	Subunit	VH gene	VL gene	CDRH3 length	Epitope type	Western blot
Kenv-1	TM	IGHV10-1	IGKV14-111	7	Linear	+
Kenv-2	TM	IGHV3-1	IGKV5-39	15	Linear*	+
Kenv-3	TM	IGHV8-8	IGKV10-94	17	Linear*	+
Kenv-4	TM	IGHV3-2	IGKV4-68	12	Conformational; postfusion	–
Kenv-6	SU	IGHV9-3	IGKV3-5	14	Conformational; prefusion	–
Kenv-7	TM	IGHV2-6-7	IGKV12-46	11	Linear	+
Kenv-8	TM	IGHV8-11	IGKV10-94	17	Linear	+
Kenv-10	SU	IGHV1-22	IGKV9-124	5	Linear	+
Kenv-14	SU	IGHV3-2	IGKV8-21	9	Linear	+

Fig. 4. mAbs with subunit and conformational specificity enable detection of Env in patient-derived samples. (**A**) Binding of mAbs to unstabilized HERV-K Phoenix Env$_{UNS}$ (Env$_{UNS}$; blue), denatured Env$_{UNS}$ (denatured Env$_{UNS}$; green), the MBP-TM$_{ECTO}$ construct (postfusion TM$_{ECTO}$; pink), and denatured MBP-TM$_{ECTO}$ (denatured TM$_{ECTO}$; orange) determined by ELISA. Each mAb was run in duplicate ($n = 2$) and each data point plotted as a circle. (**B**) Western blots using anti-Env mAbs as the primary antibody. All blots used purified, unstabilized Env$_{UNS}$, which contains both SU (~51 kDa) and TM$_{ECTO}$ (~30 kDa) bands. (**C**) Table of anti-Env mAbs found in this study. Antibodies were screened for SU or TM binding using ELISA shown in fig. S1A. Epitope type was determined using ELISAs in combination with Western blots. * = presumed linear based on Western blotting results. (**D**) Immunofluorescence staining of isolated neutrophils from either SLE, RA, or healthy donors using mAbs from this study and the commercially available TM-binding HERM-1811-5 antibody. Healthy neutrophils show no staining by any mAb.

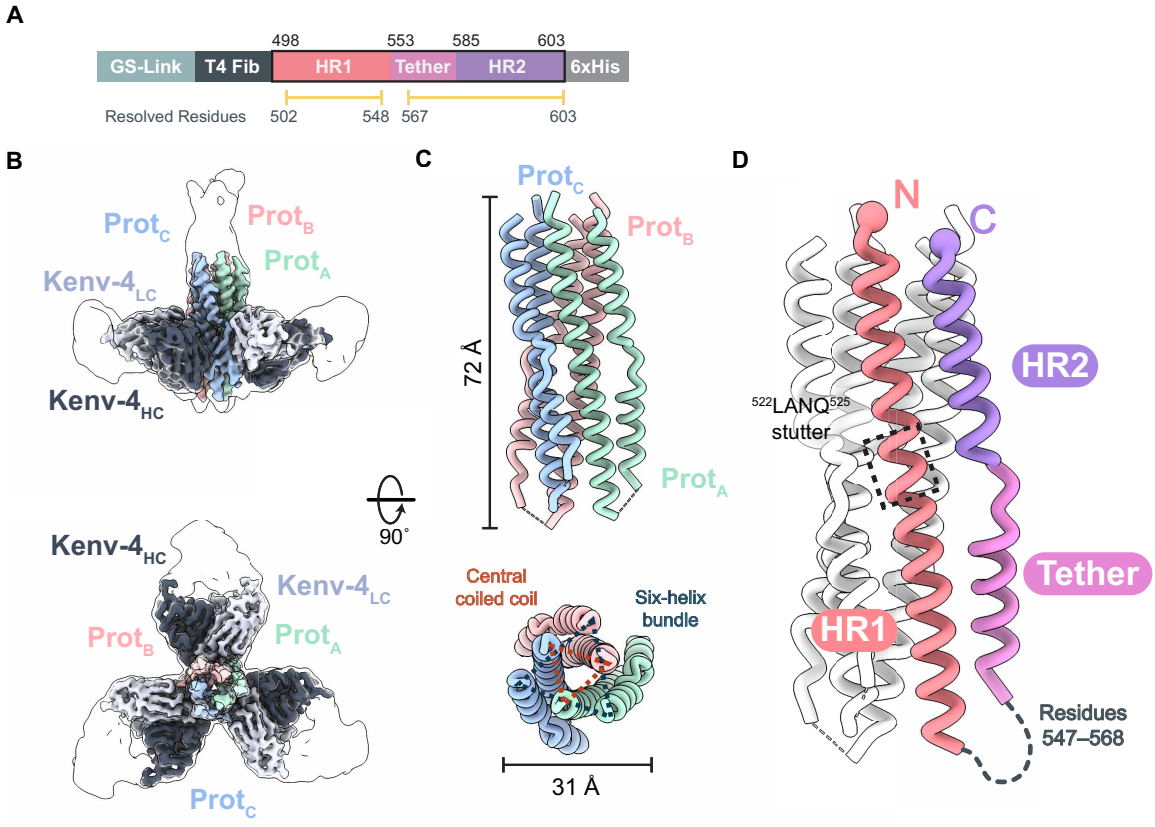

Fig. 5. Cryo-EM structure of the Kenv-4 bound postfusion HERV-K TM_{ECTO} complex reveals the 6HB architecture. (**A**) Schematic representation of the postfusion HERV-K TM_{ECTO} construct. Abbreviations: GS-link, 17-amino acid linker. (**B**) 2.8-Å resolution cryo-EM map of postfusion TM_{ECTO} trimer (colored using green, blue, and red shades) bound to three copies of the Kenv-4 Fab. A low-resolution map is overlaid and represented as a silhouette. (**C**) A ribbon representation of the postfusion TM_{ECTO}. 6HB and central coiled-coil structural features are shown using dotted triangles. (**D**) A protomer of postfusion TM_{ECTO} with domains colored as described in (A).

Env undergoes large conformational reorganizations during the pre to postfusion transition

HERV-K Env–mediated fusion requires proteolytic processing of SU and TM, a low-pH environment, and dissociation of SU from TM (*58*). The dissociation of SU from TM initiates the irreversible springing to the low-energy state, where the fusion peptide inserts into the target membrane, starting the process of membrane fusion. Alignment of the prefusion to the postfusion TM revealed two major structural rearrangements that occur around α8, which, itself, remains largely unaltered between the two conformations. The first rearrangement is the formation of the elongated HR1 helix (residues 502 to 546) by the displacement of the fusion peptide, pulling α6 and α7 away from the cell membrane. α6 and α7 are disjointed helices that form one arm of the C-shaped clamp in the prefusion conformation (fig. S7B). The HR1 central helix, initially ~30 Å in length, extends to ~67 Å, likely forming the pre-hairpin intermediate, consistent with Env rearrangements observed in HIV and murine leukemia virus (MLV) during membrane fusion (*82*, *83*). In the second rearrangement, TM reverses direction to form a hairpin. The α9 and α10 helices pack tightly along the now-extended HR1 helix, forming the tether and HR2 helices, respectively, in the postfusion structure (fig. S7C). This reorganization positions the sequence following HR2, including the unresolved membrane-spanning region at the C terminus, closer to the target membrane, driving membrane fusion (fig. S7, C and D). Residues 546 to 566, which include an intramolecular disulfide bond between $^{551}CX_7C^{559}$ and the β27 strand in the prefusion conformation, facilitate the chain reversal. We could model this region in the prefusion structure but could not resolve it in the postfusion structure, likely due to inherent flexibility.

HERV-K TM contains a unique tether helix

We manually curated nine other retroviral envelope postfusion structures from the Protein Data Bank (PDB) [HIV-1 (PDB:1I5X), SIV (PDB:1QBZ), avian sarcoma leukosis virus (PDB:4JPR), human T lymphotropic virus 1 (PDB:1MG1), porcine endogenous retrovirus (PDB:7S94), Syncytin-1 (HERV-W) (PDB:6RX1), Syncytin-2 (HERV-FRD) (PDB:6RX3), xenotropic MLV–related virus (PDB:4JGS), and Mason-Pfizer monkey virus (PDB:4JF3)] and performed sequence and structural alignments (fig. S8). All structures feature a long α helix corresponding to the HR1 region (fig. S8, B and C). However, while other retroviruses have two helices (HR1 and HR2), the postfusion HERV-K TM core exhibits three: with the additional helix located in the central tether sequence between HR1 and HR2. We have termed this third helix the tether helix (fig. S8, B and C). The HERV-K tether helix shares sequence similarity to the N termini of other retroviral HR2s, but it does not adopt the typical HR2 position (fig. S8B). Instead, it packs against the N-terminal region of the HR1 helix. The HERV-K TM HR2 sequence aligns with the C termini of other HR2 sequences rather than the entire length and structurally packs against the C-terminal region of the HR1, consistent with most other retroviral HR2s. Although we

did not model the entire HERV-K HR2 due to flexibility, the region that was modeled (residues 585 to 603) does pack similarly to the compared structures on the outside of HR1. RMSDs of the HERV-K TM with other retroviral TM (ranging from ~4 to 20 Å for all atom pairs) are provided in table S4.

Conformational mAbs define epitopes on HERV-K Env

The Kenv-6 epitope

To further define how Kenv-6 engages the Env and to validate its conformational specificity, we determined the structure of Kenv-6 Fab in complex with the stabilized prefusion Env_{ECTO} by cryo-EM. The Kenv-6–Env complex was purified by SEC and vitrified on graphene oxide–coated grids. A total of 479,625 particles from 13,141 movies were processed with CryoSPARC (*59*) to obtain a reconstruction at a 2.2-Å global resolution (figs. S9A and S12).

Three Kenv-6 Fabs bind to the trimeric prefusion Env_{ECTO}; each copy of the antibody anchors to a conformational epitope at the apex of SU (fig. S9B) and buries 569 $Å^2$ by its heavy chain and 363 $Å^2$ by its light chain. The Kenv-6 heavy chain contacts Env primarily via the complementarity determining region (CDR) H3, which forms hydrogen bonds with both side chain and backbone atoms of residues in the loops of SU proceeding β13 (residues 277 to 281), and between β14-β15 (residues 309 to 313) and β17-β18 (residues 361 to 364) (fig. S9C). The CDRH1 and CDRH2 of Kenv-6 form hydrogen bonds to R280 and S281. Light-chain CDRL1 and CDRL2 hydrogen bond to the hydroxyl oxygen on the side chains of both Y367 and E314 and the backbone oxygen of R363 (fig. S9D).

This structure confirms Kenv-6 as a truly conformation-specific antibody, engaging loops at the apex of SU, while preserving the fold of the prefusion trimer. Alignment with the unbound, apo Env reveals no meaningful structural difference. Notably, residues in the Kenv-6 epitope are broadly conserved among intact HERV-K Envs encoded in the human genome (fig. S1).

The Kenv-4 epitope

In the cryo-EM structure of the complex of the postfusion conformation of HERV-K Env TM_{ECTO} bound to Kenv-4, we observe that Kenv-4 also binds a conformational epitope but one specific to the postfusion conformation of trimeric TM. Three copies of the Kenv-4 Fab are symmetrically bound to the flexible loop (residues 581 to 585) of TM, with each Fab bridging two adjacent monomers in the postfusion conformation (fig. S10B). The heavy chain of Kenv-4 buries 522 $Å^2$ of surface area on the postfusion TM, while the light chain buries 386 $Å^2$. The Kenv-4 heavy chain engages two adjacent monomers, while its light chain interacts with only one monomer. The heavy chain interaction is mediated by CDRH1 and CDRH2 (fig. S10D). Here, residue D32 of the CDRH1 forms salt bridges to R539 on one monomer ($Prot_A$) and H571 on the adjoining monomer ($Prot_B$); in the complex, three copies of Kenv-4 make three such interactions around the trimer. Light chain binding is only mediated by CDRL1 with six hydrogen bonds and Y70 in framework 3 hydrogen binding to E583 (fig. S10C). The postfusion conformation-specific Kenv-4 did not bind with neutrophils from either of the patient samples evaluated here, although other TM-binding mAbs did (Fig. 4B).

DISCUSSION

HERVs, particularly the HERV-K (HML-2) family, are ancient retroviral elements scattered throughout the human genome (*6*, *8*, *12*). Although previously considered silent "junk" DNA, HERV-K insertions retain ORFs and can express proteins, including the Env. RNA transcripts and protein expression of Env have been demonstrated in various cancer tissues, including but not limited to breast cancer, ovarian cancer, leukemia, and melanoma (*15*, *17*, *21*, *22*, *84*, *85*). Expression of HERV-K Env is also associated with RA, SLE, T1D, multiple sclerosis, and various other autoimmune and neurodegenerative disorders (*11*, *30*, *33*, *86*–*88*).

Beyond expression, Env has been shown to exhibit functional activity. It may bind to CD98HC (SLC3A2), an extracellular membrane–bound protein involved in regulating cell growth, proliferation, and tumor metabolism (*35*, *89*, *90*). Further, Env expressed by the K108 locus on human chromosome 7 is fusogenic (*91*) and promotes melanoma cell-cell fusion in vitro (*20*). Further, HERV-K Env expression elicits a humoral immune response, including anti-Env antibody generation in cancers (*15*, *17*, *92*) and autoimmune disorders, which may correlate with disease progression (*7*, *33*, *36*–*38*, *93*). Immune complexes formed between Env and these antibodies can stimulate proinflammatory responses, contributing to the disease pathogenesis (*7*).

Despite their biological importance in multiple human disease states, no structures of any HERV envelope trimer have been determined. Without a structural framework, it remains unclear how HERV-K Env interacts with cellular factors to trigger fusion or downstream cell signaling, how Env is recognized or neutralized by antibodies, or how to rationally design targeted therapeutic interventions and Env-based diagnostics.

In this work, we present high-resolution cryo-EM structures of the stabilized HERV-K Env ectodomain trimer in prefusion (2.2-Å resolution), antibody-bound prefusion (2.2-Å resolution), and antibody-bound postfusion (2.8-Å resolution) conformations. Although the conformations of Env on cell surfaces during disease states are not yet characterized, one may expect from our understanding of the metastability of viral glycoproteins that both pre and postfusion structures may exist on the cell surface and both be relevant for antibody recognition.

The overall structure of the prefusion HERV-K Env diverges from the primate lentivirus envelope proteins solved previously, with distinct folds of the SU subunits and at least 23-Å RMSD in the assembled trimer from other known structures. The HERV-K Env trimer adopts a narrower profile than HIV-1 and SIV and heavily incorporates β strands rather than α helices into the SU subunit. The five-stranded β sheet at the core of HERV-K Env SU, however, is similar to the SU core domain of Syncytin-2, a former endogenous retrovirus protein co-opted for human placental function (*76*). In contrast, the TM subunit of HERV-K, the core molecular machinery that guides 6HB formation and membrane fusion, bears more structural similarity to its equivalent gp41 subunit in HIV-1 and SIV. Within the TM subunit however, key features unique to HERV-K were revealed including a CX_7C sequence motif found in betaretroviral envelopes (*48*) and the tether helix between HR1 and HR2 in the postfusion conformation. Another distinction is that HERV-K Env bears only a moderate glycan shield compared to the lentiviral envelopes of HIV-1 or SIV (23 versus 53 amino acids per glycan). This results in more accessible and conserved surfaces of vulnerability, particularly in SU, for targeting by anti-Env antibodies.

While this manuscript was under review, a preprint describing the prefusion structure of the HERV-K Env determined using the full-length, unstabilized consensus Env was posted (*94*). That study resolves the ectodomain in a prefusion conformation highly consistent

with our Env structures, further validating that our stabilized Env_{ECTO} adopts the native prefusion fold.

In this work, we also generated a panel of mAbs to support these structural studies and to enable subsequent interrogation of Env conformations in cells and tissues, and explore future diagnostic and therapeutic use. These mAbs target SU and TM subunits include both linear and conformational epitope specificity. As one example, mAb Kenv-6, solved in complex with prefusion Env by cryo-EM, preferentially recognizes the prefusion conformation of Env, and binds a conformational epitope at the apex of SU near the presumed receptor binding site. Kenv-6 does not alter the prefusion fold of Env and serves as a reliable probe for assessing native Env expression and folding in biological contexts. Kenv-6 strongly stains neutrophils isolated from both RA and SLE patients (Fig. 4B), a cell type previously reported to express Envs from both type 1 (K102) and type 2 (K108) HERV-K insertions in these diseases (*32*, *33*).

Another mAb, Kenv-4, is specific for the postfusion conformation of Env and was critical for resolving the structure of the postfusion HERV-K Env TM trimer. Kenv-4 did not stain autoimmune patient neutrophils. Notably, other TM-specific mAbs do stain these cells, suggesting that postfusion conformation Env may still be present as well as the prefusion conformation. We note that staining could differ between autoimmune and cancer contexts: The tumor microenvironment is characterized by more acidic pH due to the accumulation of metabolic waste (*95*, *96*), which may promote the acidic pH–driven (*58*, *97*) rearrangement of Env to its postfusion conformation. Antibody tools developed here allow for the exploration of conformational landscapes and their implications for immune recognition.

The structures, stabilized antigens, and antibodies presented here offer the blueprints and valuable reagents that facilitate detection of HERV-K expression and investigation of its roles in human disease states. HERV-K Env expression is observed in autoimmunity; five anti-Env antibodies described here stain human neutrophils from autoimmune disease patient samples but not neutrophils from healthy humans. HERV-K is also expressed in cancers and has garnered substantial interest as a possible neoantigen or tumor-associated antigen (*23*, *98*). Several strategies targeting Env in cancer have shown promise: An anti-Env mAb termed 6H5 inhibited growth and induced apoptosis of breast cancer cells in vitro in a dose-dependent manner. Used in vivo, mice bearing xenograft tumors displayed significantly reduced growth after 6H5 treatment compared to an immunoglobulin G (IgG) control (*40*). Further, a nanobody targeting Env was reported to induce antibody-dependent cellular cytotoxicity in lymphoma cell lines and can be internalized by Env-expressing cells, warranting further exploration into anti-Env antibody drug conjugates (*99*). Moreover, CAR-T cells engineered to target HERV-K Env have been effective in lysing breast cancer and melanoma tumors, inhibiting cell proliferation, and preventing metastasis in vitro and in vivo (*41*, *42*). The GNK-301 mAb (GeNeuro) binds to a linear epitope located on the β14 strand at top of Env SU, blocks its interaction with CD98HC, and mitigates Env-related neurotoxicity in ALS (*35*). Structural features at the apex of SU, including β14 and adjacent loops, are plausible binding sites, but structures of the Env-CD98HC are required to definitively map the interaction. Our Kenv-6 mAb also binds to the apex of SU in proximity to the same β14 strand, although its functional effects remain to be explored.

Previous investigations to determine whether there are autoantibody responses against Env in disease have largely used linear peptides or bacterially expressed Env, thereby failing to capture antibodies that target conformational epitopes or intact, glycosylated Env (*36*, *37*, *93*), and were performed in the absence of structural information on Env. Here, we present fully folded, glycosylated, and structurally validated Env constructs that can be used for functional assays, serological screens, and antibody discovery efforts. The cryo-EM structures of HERV-K Env described in this study now provide the blueprint for identifying immunodominant epitopes and dissecting its roles in immunity, signaling, and disease pathogenesis. Further, the mAbs introduced here can be used to detect or target diseased cells, or neutralize Env-mediated effects in disease, either by outcompeting patient-derived antibodies or by blocking binding to surface receptors. This study establishes the structural framework for exploring the functions of the many HERV-K *env* loci and their gene products in disease pathogenesis and provides essential tools needed for understanding Env biology and the development of novel immunotherapies, diagnostics, and vaccines.

MATERIALS AND METHODS

Plasmids and cloning

The genes of HERV-K Env Phoenix consensus proteins were initially codon-optimized, synthesized, and cloned into a phCMV mammalian expression vector (Addgene) using HiFi DNA assembly (New England Biolabs). The ectodomain construct (Env_{ECTO}) was generated by removing the native signal sequence (residues 1 to 96) and transmembrane region onward (residues 632 to 699). Stabilizing point mutations V437C and V498C were introduced using site-directed mutagenesis. Stabilized Env_{ECTO} was subcloned into the insect cell expression vector pMT-puro (Addgene). A codon-optimized HERVK-TM (residues 498 to 603) sequence was synthesized by GenScript and subcloned into the pET-46 vector (Addgene) using HiFi DNA assembly (New England Biolabs).

Cells

Drosophila S2 cells were cultured at 27°C in stationary flasks without CO_2 in complete Schneider's *Drosophila* medium (Gibco) supplemented with 10% heat-inactivated fetal bovine serum (FBS) and 1% penicillin-streptomycin [(100 U/ml) penicillin and (100 μg/ml) streptomycin] or in serum-free Insect Xpress Medium (Lonza). Stable cell lines were adapted to Insect Xpress medium and maintained with shaking at 27°C.

HEK293T (human embryonic kidney epithelial) cells were grown in Dulbecco's modified Eagle's medium (Thermo Fisher Scientific) supplemented with 10% FBS (Thermo Fisher Scientific) and antibiotics at 37°C in 5% CO_2. ExpiCHO cells were maintained in ExpiCHO Expression medium (Gibco) in a humidified incubator at 37°C with 8% CO_2.

HERV-K Env_{ECTO} expression and purification

To generate *Drosophila* S2 stable cell lines, S2 cells were cotransfected with a pBLAST Furin protease expression vector and the pMT-puro stabilized Env_{ECTO} construct containing a C-terminal enterokinase cleavage sequence and a flexible 4xGly-Gly-Ser linker to the T4 fibritin trimerization domain. This construct also contains an HRV 3C cleavage sequence and a twin-strep-tag (IBA Biosciences). Transfected cells were grown and selected using puromycin (6 μg/ml) and 25 blasticidin (μg/ml). Stable cell lines were expanded and adapted to Lonza Insect Xpress medium and maintained with shaking at 27°C.

S2 cells were grown to a density of 1×10^7 cells/ml, and protein expression was induced using 500 μM $CuSO_4$. The cells were removed after 5 to 7 days via centrifugation at 6000 *g*, and the resulting media were treated with BioLock (IBA Lifesciences, Göttingen, Germany).

Protein was purified from the media by Strep-Tactin affinity chromatography using a StrepTrap XT column (Cytiva). The column was washed with EQ buffer [25 mM tris-HCl and 150 mM NaCl (pH 8.0)] and then eluted with elution buffer [25 mM tris-HCl, 150 mM NaCl, and 50 mM biotin (pH 8.0)] The resulting protein was further purified by SEC using a Superdex 200 increase 10/300 GL column (Cytiva) in tris-buffered saline (TBS) (pH 8.0). Fractions containing HERV-K Env_{ECTO} trimer were pooled and concentrated. Protein was either flash frozen for storage or used immediately.

SDS–polyacrylamide gel electrophoresis

A total of 2 μg of HERV-K Env proteins were incubated with a 4× LDS sample running buffer with (reducing) or without (nonreducing) 5 mM DTT. Samples were boiled at 95°C for 5 min and run on a 4 to 15% stain-free gel (Bio-Rad). Gels were imaged using a ChemiDoc MP Imaging System (Bio-Rad).

T_m analysis

Size exclusion–purified HERV-K Env proteins were diluted to a concentration of 0.3 mg/ml. Glass capillaries were loaded with 10 μl of protein. The Prometheus Panta (NanoTemper) was used to measure thermal stability by nano differential scanning fluorimetry using a thermal ramp with a range of 25° to 98°C. Ultraviolet (UV) absorbance at a wavelength of 330 nm was measured over the temperature range, and inflection points of the first derivative were used to determine the T_m for each protein. Samples were measured and analyzed in triplicate.

pH-dependent T_m analysis

Size exclusion–purified HERV-K Env proteins were diluted to a concentration of 0.3 mg/ml using buffers in pH: 7.5 (50 mM tris and 150 mM NaCl), 7.0 [10 mM phosphate-buffered saline (PBS) and 150 mM NaCl], 6.5 (50 mM MES and 150 mM NaCl), 6.0 (50 mM MES and 150 mM NaCl), 5.5 (50 mM sodium acetate and 150 mM NaCl), and 5.0 (50 mM sodium acetate and 150 mM NaCl). Buffers were adjusted to respective pHs using HCl or NaOH. Glass capillaries were loaded with 10 μl of protein in pH buffer. The Prometheus Panta (NanoTemper) was used to measure thermal stability by nano differential scanning fluorimetry using a thermal ramp with a range of 25°to 98°C. UV absorbance at a wavelength of 330 nm was measured over the temperature range, and inflection points of the first derivative were used to determine the T_m for each protein. Samples were measured and analyzed in triplicate.

Expression and purification of HERV-K post fusion TM_{ECTO} trimer

The DNA sequence of HERV-K TM (residues 498 to 603) was codon optimized for expression in *E. Coli*. It was synthesized by GenScript and subcloned into pET-46 construct containing an MBP tag, $(GGSG)_2$ linker, HRV 3C protease cleavage site, a flexible GS linker, T4 fibritin trimerization domain at the N terminus, a six-his tag at the C terminus.

A single plasmid containing HERV-K-TM was transformed into Rosetta 2 (DE3) Singles Competent Cells - Novagen (Millipore Sigma), plated onto LB-ampicillin agar plates, and incubated overnight at 37°C. A single colony was used to prepare an overnight culture in 25-ml LB medium supplemented with ampicillin (100 μg/ml) and chloramphenicol (34 μg/ml). The cells were used to inoculate 1-liter cultures supplemented with ampicillin (100 μg/ml) for 4 hours. At an optical density at 600 nm (OD_{600}) between 0.8 and 1.0, the cells were induced with 0.5 mM isopropyl-β-D-thiogalactopyranoside and shaken overnight at 16°C.

The cells were harvested by centrifugation at 12°C for 25 min and 6000*g*. The resulting pellets were resuspended in buffer A [20 mM sodium phosphate (pH 7.4), 500 mM Nacl, and 30 mM imidazole]. One microliter of Benzonase nuclease was added, and the suspension was lysed using an M-110P microfluidizer, Microfluidics). After clarification, the supernatant was filtered through a 0.22-μm filter. The cell lysate was loaded into a HisTrap HP 5-ml column (Cytiva). The column was first washed with buffer A and then eluted with buffer B [20 mM sodium phosphate (pH 7.4), 500 mM Nacl, and 500 mM imidazole] for five column volumes. Fractions containing the target protein were pooled, concentrated, and passed over a Superdex 200 increase 10/300 GL column (Cytiva) at a flow rate of 0.5 ml/min using TBS buffer [50 mM tris (pH 7.5) and 150 mM NaCl]. The peak fractions containing HERV-K TM_{ECTO} were pooled.

Mouse immunization

Unstabilized HERV-K Phoenix envelope ectodomain with a C-terminal twin strep-tag (IBA Biosciences) was produced in *Drosophila* S2 and affinity purified via Strep-Tactin affinity chromatography using a StrepTrap XT column (Cytiva). The affinity-purified protein was then run on a Superdex 200 increase 10/300 GL column (Cytiva) in TBS pH 8.0. Fractions corresponding to a monomeric SU + TM were collected and concentrated. Eight-week-old female BALB/c mice (the Jackson Laboratory) were immunized with 20 μg of this purified Phoenix envelope ectodomain monomer and 2.5 μg of saponin/MPLA nanoparticles (SMNP) adjuvant (gift of D. Irvine, MIT and Scripps Research) (*100*) subcutaneously in each leg. The mice were subsequently boosted with an additional 20 μg of protein and 2.5 μg of adjuvant in each leg 4 weeks after initial immunization. All study protocols and procedures were approved by the Institutional Animal Care and Use Committee at the La Jolla Institute for Immunology (protocol # AP00001328).

PC isolation

Five days postboost, splenocytes were subject to two-step magnetic cell sorting to isolate plasma cells (PCs). After RBC lysis, non-PCs were depleted (Miltenyi Biotec) followed by enrichment of PCs with an EasySep Mouse CD138 Positive Selection kit (Stemcell Technologies).

Antibody discovery

Screening with Beacon

Enriched PCs were loaded onto OptoSelect 11 K chips (Bruker Cellular Analysis, BCA), wherein they were isolated as single cells in nanoliter pens using OEP light cages. Cells were screened in a 30-min time course assay for secretion of antibodies that bound to streptavidin beads (Spherotech) coated with biotinylated HERV-K Phoenix Env_{UNS} ectodomains (5 μg/ml). Secreted antibodies were detected with goat anti-mouse IgG (H + L)–Alexa Fluor 594 (1 μg/ml; Invitrogen), which was added to the cell culture media used to resuspend the antigen-coated beads.

Cloning

On-chip cDNA synthesis was carried out using the BCA OptoSeq BCR kit. First-strand reaction products were exported on mRNA

capture beads and deposited into individual wells of a 96-well plate where total cDNA was amplified using Platinum SuperFi II polymerase (Invitrogen). After enzymatic cleanup, antibody heavy and light chain variable domains were amplified Platinum TaqII HotStart polymerase (Invitrogen) using the BCR Fwd primer from BCA and reverse primers recognizing the constant domain of the mouse Ig heavy chain and kappa light chain (19716372). The resulting polymerase chain reaction (PCR) products were Sanger sequenced and analyzed using the PipeBio cloud platform. VH and VL domains were cloned into linearized phCMV antibody expression vectors (human IgG1 kappa light chain) using Gibson assembly (NEB) according to the manufacturer's directions. Ligation reactions were transformed into 5-alpha F'Iq competent *E. coli* cells (NEB). QIAprep 96 Turbo Miniprep kits (Qiagen) were used to isolate plasmids according to the manufacturer's instructions. Briefly, S block wells containing 1.1 ml of LB media spiked with antibiotics were inoculated with single colonies and incubated overnight at 37°C with agitation. DNA extraction was carried out with Qiagen buffer solutions and protocols. Plasmids were sequenced to ensure that the genes were in-frame, and the cloned heavy and light chain variable domains were compared to PCR sequences.

Expression and purification of HERV-K Env antibodies

ExpiCHOs were cotransfected with heavy (8 μg DNA/ml cells) and light chain (7 μg DNA/ml cells) plasmid pairs using the ExpiFectamine CHO transfection kit (Thermo Fisher Scientific). Cells were grown shaking at 37°C with 8% CO_2. Cells were spun down at 4000 *g* after 7 days and Protein A MagBeads (GenScript) were incubated with media overnight at 4°C. Antibodies were purified and eluted in 0.1 M glycine (pH 2.0) using the AmMag SA Plus system (GenScript). Eluted antibodies were then dialyzed in PBS (pH 7.4) overnight at 4°C.

ELISA screening

To determine the subunit specificity of anti-Env antibodies, 96-well clear flat-bottom plates (Corning) were coated with 100 ng of purified Env_{UNS} or postfusion MBP-TM_{ECTO} for 2 hours at 25°C. To determine the conformational specificity of anti-Env antibodies, consensus envelope ectodomain or postfusion MBP-TM_{ECTO} was heated with 5 mM DTT at 95°C for 10 min before coating with 100 ng of protein onto the 96-well plate for 2 hours at 25°C. The wells were then blocked for 1 hour with 125 μl of PBS buffer containing 3% casein. Purified anti-Env antibodies (1 μg/ml) in blocking buffer were added to the wells and incubated overnight at 4°C. The wells were washed three times with PBS + 0.1% Tween-20 (PBST), and goat anti-human IgG (H + L) cross-absorbed or goat anti-mouse IgG (H + L) secondary antibody conjugated with horseradish peroxidase (HRP, Invitrogen) diluted 1:7500 in blocking buffer was added on for 1 hour at 25°C. The wells were washed five times with PBST. Trimethylboron ELISA substrate (Thermo Fisher Scientific) was then added to each well and developed for 5 min before quenching the reaction. ODs were measured using a plate reader reading at 450 nm (Tecan).

Western blot

Protein samples were run on an SDS-PAGE gel as described above. The samples were transferred onto a polyvinylidene difluoride membrane using a wet tank system. The membrane was blocked in 5% blotting-grade blocker (Bio-Rad) PBS for 1 hour at 25°C. The membranes were then incubated with anti-Env antibodies at 0.1 to 1 μg/ml in the blocking buffer overnight at 4°C. The HERM-1811-5 antibody (Austral Biologics), was incubated with membrane at a 1:1000 dilution. Three washes were performed using PBST. Goat anti-human IgG (H + L) cross-absorbed secondary antibody conjugated with HRP (Invitrogen) at a dilution of 1:10,000 was added to the membrane for 1 hour at 25°C. The sample with HERM-1811-5 had goat anti-mouse IgG (H + L) added also at a 1:10,000 dilution. The membrane was developed after three more washes in PBST using Super-Signal West Pico PLUS Chemiluminescent Substrate (Thermo Fisher Scientific). Blots were imaged and analyzed using a ChemiDoc MP Imaging System (Bio-Rad).

Neutrophil staining with Kenv antibodies

Freshly isolated neutrophils were incubated for 30 min at 37°C in 96-well glass bottom plates (Cellvis) precoated with poly-L-lysine (Millipore-Sigma). The adherent cell populations were fixed with 4% paraformaldehyde solution for 20 min, followed by two sequential washes with PBS. Cellular permeabilization was performed using 0.1% Triton X-100 in PBS for 10 min followed by three successive washes with PBS. To minimize nonspecific binding, neutrophils were blocked using 10% normal mouse and/or goat serum in BlockAid solution with anti-human FcγRII antibody overnight at 4°C. Subsequently, neutrophils were incubated with a 1:50 dilution of anti-Env antibodies, followed by three consecutive washes with PBS. The specimens were then labeled with goat anti-mouse IgG secondary antibody conjugated with Alexa Fluor 647 (red). Control samples comprised cells stained without primary antibody or with only secondary antibodies. Nuclear DNA was visualized with either 4′,6-diamidino-2-phenylindole or Hoechst33342. Microscopic images were acquired at 40×, 60×, or 100× magnification using a Keyence BZ-X800 Fluorescence microscope and processed using BZ-X800 Analyzer software.

Samples were obtained through the University of Washington Rheumatology Biorepository with approval of the Institutional Review Board (STUDY00006196). Informed written consent was obtained from all participants according to the Declaration of Helsinki.

Fab complexing

IgG digestion

Kenv-4 and Kenv-6 IgGs were incubated with 20% w/w of FabALACTICA (gift of D. Fremont, Washington University in St. Louis) for 16 to 18 hours at 37°C to generate cleaved Fab and Fc domains. Protein A agarose beads (Purolite) were added to solution and rocked for 1 hour at 25°C to capture Fc. The bead mixture was then spun down at 200*g* for 5 min, and the Protein A beads were removed from supernatant containing Fabs.

Complexing Env_{ECTO} trimer with Kenv-6 Fab

SEC-purified HERV-K Env_{ECTO} was incubated with Kenv-6 Fab overnight with a molar ratio of 1:3. Intact complexes were purified using the Superdex 200 increase 10/300 GL column (Cytiva) to remove unbound Fab. Fractions containing Env-Fab complexes were concentrated and used the same day.

Complexing HERV-K-TM trimer with Kenv-4 Fab

Purified MBP-TM_{ECTO} was incubated with Kenv-4 Fab overnight with a molar ratio of 1:3. Then, the complex was digested with HRV 3C protease at 4°C overnight. The reaction was passed on to a Superdex 6 increase 10/300 GL column (Cytiva) in the TBS buffer to purify the Fab bound HERVK-TM_{ECTO}.

Negative stain-EM grid preparation, data collection, and processing

Size exclusion–purified HERV-K Env constructs were diluted to a concentration of 0.02 mg/ml in PBS. Protein was applied to a copper 400-mesh carbon film grid and stained with 2% uranyl acetate. Negative stain movies were collected on a 300-kV Titan Halo (Thermo Fisher Scientific) with a K3 direct electron detector (Gatan). Images were recorded at a defocus range of −2 to −3 μm with a nominal magnification of 18,000× with a pixel size of 1.7 Å. Movies were motion and contrast transfer function (CTF) corrected. Particle picking was performed with the blob picker with the particle diameter range of 100 to 250 Å. Multiple rounds of two-dimensional (2D) classification were performed to yield the final classes shown in fig. S3 (C and D). All data were processed with CryoSPARC (Structura Biotechnology Inc.) (*59*).

Cryo-EM grid preparation and data collection

Size exclusion–purified HERV-K Env_{ECTO} at a concentration of 0.192 mg/ml and HERV-K Env_{ECTO} Kenv-6 complexes at a concentration of 0.179 mg/ml were applied to homemade graphene oxide grids that were prepared using a previously described protocol (*101*). Purified HERV-K TM_{ECTO} Kenv-4 complexes at a concentration of 0.68 mg/ml were applied to an UltrAuFoil R1.2/1.3 300 mesh grid. Samples were plunge-frozen in liquid ethane with an FEI vitrobot Mark IV (Thermo Fisher Scientific) in 100% humidity and 4°C with 6- to 8-s blotting time. Movies were collected on a 300-kV Titan Krios (Thermo Fisher Scientific) with a K3 direct electron detector (Gatan) and BioQuantum K3 Imaging Filter (Gatan) with a slit width of 10 eV. Images were recorded at a defocus range of −0.8 to −2 μm with a nominal magnification of 130,000×, resulting in a pixel size of 0.66 Å. Details of the data collection conditions are listed in table S1.

Cryo-EM data processing

The flowcharts for data processing of the apo Env_{ECTO} trimer, Kenv-6 bound Env_{ECTO} trimer and Kenv-4 bound HERV-K-TM_{ECTO} trimer are presented in figs. S11 to S13, respectively. All movies were imported into CryoSPARC (Structura Biotechnology Inc.) (*59*) to perform patch motion correction and patch CTF estimation.

Image processing for apo Env_{ECTO} trimer

A total of 8603 movies were motion and CTF corrected. Particle picking was performed with the blob picker with the particle diameter range of 100 to 250 Å. Multiple rounds of 2D classification were performed to remove junk particles. An ab initio reconstruction was generated with an initial set of particles, which were then used for nonuniform refinement with C3 symmetry imposed. Further classification in 3D using heterogenous refinement and 3D classification jobs removed classes lacking clear secondary-structure features. CTF polishing of the final set of particles and running a final nonuniform refinement job yielded a 2.2-Å resolution map.

Image processing for Env_{ECTO} trimer with Kenv-6 Fab

Micrographs were curated using a 5.5-Å CTF cutoff. Particle picking was performed with the blob picker with the particle diameter range of 100 to 300 Å. Multiple rounds of 2D classification were performed to remove junk particles. An ab initio reconstruction was generated with an initial set of particles that were then further classified in 3D using heterogenous refinement and 3D classification jobs. The antibody Fab constant regions were masked out because of observed flexibility, and a focused refinement was performed on the Fab variable region and the Env trimer with C3 symmetry imposed. Particles were then symmetry expanded and further 3D classified in C1, yielding two good classes. Duplicated particles from the largest class were then removed before CTF polishing of particles and running a local refinement job, which yielded a 2.2-Å resolution map.

Image processing for HERV-K-TM_{ECTO} trimer with Kenv-4

Micrographs were curated using a 20-Å CTF cutoff. Particle picking was performed with the blob picker with the particle diameter range of 100 to 160 Å. Multiple rounds of 2D classification were performed to remove junk particles. All the particles were subjected to ab initio reconstruction and homogenous refinement with C1 symmetry. After symmetry expansion with C3 symmetry, duplicated particles were removed. 3D classification was performed to separate the particles with different numbers of Fabs. The three-Fab bound class with the greatest number of particles was selected for the final refinement. A focus mask with the TM trimer and the variable region of the Fab was generated on the basis of ab initio map and applied in the local refinement job yielding a 2.8-Å resolution map.

Model building

To obtain a starting model for the prefusion structures, automated model building with sharpened maps using ModelAngelo (*102*) was performed, which was further manually built in Coot 0.9.8.7 (*103*, *104*). Structure predictions of the Fabs and postfusion HERV-K TM were performed with the AlphaFold3 server (*105*). The predicted structures were docked into ChimeraX (*56*). The deepEMEnhanced (*106*) maps were used for manual model building. Multiple rounds of Phenix.real_space_refine (*107*) and manual model correction in Coot were performed. The quality of the refined models was analyzed by MolProbity (*108*) integrated in Phenix, with statistics reported in table S1.

Supplementary Materials

This PDF file includes:

Figs. S1 to S14
Tables S1 to S4
Raw SDS-PAGE and Western Blot Gel Images
References

REFERENCES AND NOTES

1. J. Paces, A. Pavlícek, V. Paces, HERVd: Database of human endogenous retroviruses. *Nucleic Acids Res.* **30**, 205–206 (2002).
2. B. Xue, L. A. Sechi, D. J. Kelvin, Human endogenous retrovirus K (HML-2) in health and disease. *Front. Microbiol.* **11**, 1690 (2020).
3. P. N. Nelson, P. R. Carnegie, J. Martin, H. Davari Ejtehadi, P. Hooley, D. Roden, S. Rowland-Jones, P. Warren, J. Astley, P. G. Murray, Demystified. Human endogenous retroviruses. *Mol. Pathol.* **56**, 11–18 (2003).
4. A. Flockerzi, A. Ruggieri, O. Frank, M. Sauter, E. Maldener, B. Kopper, B. Wullich, W. Seifarth, N. Müller-Lantzsch, C. Leib-Mösch, E. Meese, J. Mayer, Expression patterns of transcribed human endogenous retrovirus HERV-K(HML-2) loci in human tissues and the need for a HERV transcriptome project. *BMC Genomics* **9**, 354 (2008).
5. C. Yang, X. Guo, J. Li, J. Han, L. Jia, H.-L. Wen, C. Sun, X. Wang, B. Zhang, J. Li, Y. Chi, T. An, Y. Wang, Z. Wang, H. Li, L. Li, Significant upregulation of HERV-K (HML-2) transcription levels in human lung cancer and cancer cells. *Front. Microbiol.* **13**, 850444 (2022).
6. R. P. Subramanian, J. H. Wildschutte, C. Russo, J. M. Coffin, Identification, characterization, and comparative genomic distribution of the HERV-K (HML-2) group of human endogenous retroviruses. *Retrovirology* **8**, 90 (2011).
7. M. Tokuyama, B. M. Gunn, A. Venkataraman, Y. Kong, I. Kang, T. Rakib, M. J. Townsend, K. H. Costenbader, G. Alter, A. Iwasaki, Antibodies against human endogenous retrovirus K102 envelope activate neutrophils in systemic lupus erythematosus. *J. Exp. Med.* **218**, e20191766 (2021).
8. M. Tokuyama, Y. Kong, E. Song, T. Jayewickreme, I. Kang, A. Iwasaki, ERVmap analysis reveals genome-wide transcription of human endogenous retroviruses. *Proc. Natl. Acad. Sci. U.S.A.* **115**, 12565–12572 (2018).

9. L. Lavie, M. Kitova, E. Maldener, E. Meese, J. Mayer, CpG methylation directly regulates transcriptional activity of the human endogenous retrovirus family HERV-K(HML-2). *J. Virol.* **79**, 876–883 (2005).
10. Z. Salavatiha, R. Soleimani-Jelodar, S. Jalilvand, The role of endogenous retroviruses-K in human cancer. *Rev. Med. Virol.* **30**, e2142 (2020).
11. N. Grandi, E. Tramontano, HERV envelope proteins: Physiological role and pathogenic potential in cancer and autoimmunity. *Front. Microbiol.* **9**, 462 (2018).
12. M. Garcia-Montojo, T. Doucet-O'Hare, L. Henderson, A. Nath, Human endogenous retrovirus-K (HML-2): A comprehensive review. *Crit. Rev. Microbiol.* **44**, 715–738 (2018).
13. R. F. Downey, F. J. Sullivan, F. Wang-Johanning, S. Ambs, F. J. Giles, S. A. Glynn, Human endogenous retrovirus K and cancer: Innocent bystander or tumorigenic accomplice? *Int. J. Cancer* **137**, 1249–1257 (2015).
14. R. Contreras-Galindo, M. H. Kaplan, P. Leissner, T. Verjat, I. Ferlenghi, F. Bagnoli, F. Giusti, M. H. Dosik, D. F. Hayes, S. D. Gitlin, D. M. Markovitz, Human endogenous retrovirus K (HML-2) elements in the plasma of people with lymphoma and breast cancer. *J. Virol.* **82**, 9329–9336 (2008).
15. F. Wang-Johanning, M. Li, F. J. Esteva, K. R. Hess, B. Yin, K. Rycaj, J. B. Plummer, J. G. Garza, S. Ambs, G. L. Johanning, Human endogenous retrovirus type K antibodies and mRNA as serum biomarkers of early-stage breast cancer. *Int. J. Cancer* **134**, 587–595 (2014).
16. J.-O. Jo, Y.-J. Kang, M. S. Ock, K. S. Song, M.-J. Jeong, S.-J. Jeong, Y. H. Choi, E.-J. Ko, S.-H. Leem, S. Kim, H.-S. Kim, H.-J. Cha, Expression profiles of HERV-K Env protein in normal and cancerous tissues. *Genes Genomics* **38**, 91–107 (2015).
17. F. Wang-Johanning, J. Liu, K. Rycaj, M. Huang, K. Tsai, D. G. Rosen, D. T. Chen, D. W. Lu, K. F. Barnhart, G. L. Johanning, Expression of multiple human endogenous retrovirus surface envelope proteins in ovarian cancer. *Int. J. Cancer* **120**, 81–90 (2007).
18. M. Natoli, J. Gallon, H. Lu, A. Amgheib, D. J. Pinato, F. A. Mauri, T. Marafioti, A. U. Akarca, I. Ullmo, J. Ip, E. O. Aboagye, R. Brown, A. Karadimitris, S. Ghaem-Maghami, Transcriptional analysis of multiple ovarian cancer cohorts reveals prognostic and immunomodulatory consequences of ERV expression. *J. Immunother. Cancer* **9**, e001519 (2021).
19. T. A. Wallace, R. F. Downey, C. J. Seufert, A. Schetter, T. H. Dorsey, C. A. Johnson, R. Goldman, C. A. Loffredo, P. Yan, F. J. Sullivan, F. J. Giles, F. Wang-Johanning, S. Ambs, S. A. Glynn, Elevated HERV-K mRNA expression in PBMC is associated with a prostate cancer diagnosis particularly in older men and smokers. *Carcinogenesis* **35**, 2074–2083 (2014).
20. G. Huang, Z. Li, X. Wan, Y. Wang, J. Dong, Human endogenous retroviral K element encodes fusogenic activity in melanoma cells. *J. Carcinog.* **12**, 5 (2013).
21. S. Depil, C. Roche, P. Dussart, L. Prin, Expression of a human endogenous retrovirus, HERV-K, in the blood cells of leukemia patients. *Leukemia* **16**, 254–259 (2002).
22. T. Li, K. Qian, J. Han, Y. Liu, L. Jia, X. Wang, T. Li, B. Zhang, J. Li, H. Li, L. Dou, L. Li, Higher expression of human endogenous retrovirus-K was observed in peripheral B lymphocytes of leukemia and lymphoma patients. *AIDS Res. Hum. Retroviruses* **40**, 268–279 (2024).
23. C. Li, Q. Qian, C. Yan, M. Lu, L. Li, P. Li, Z. Fan, W. Lei, K. Shang, P. Wang, J. Wang, T. Lu, Y. Huang, H. Yang, H. Wei, J. Han, J. Xiao, F. Chen, H. Atlas, HervD Atlas: A curated knowledgebase of associations between human endogenous retroviruses and diseases. *Nucleic Acids Res.* **1**, 13–14 (2013).
24. F. Zhou, M. Li, Y. Wei, K. Lin, Y. Lu, J. Shen, G. L. Johanning, F. Wang-Johanning, Activation of HERV-K Env protein is essential for tumorigenesis and metastasis of breast cancer cells. *Oncotarget* **7**, 84093–84117 (2016).
25. C. Lemaître, J. Tsang, C. Bireau, T. Heidmann, M. Dewannieux, A human endogenous retrovirus-derived gene that can contribute to oncogenesis by activating the ERK pathway and inducing migration and invasion. *PLOS Pathog.* **13**, e1006451 (2017).
26. M. Li, L. Radvanyi, B. Yin, K. Rycaj, J. Li, R. Chivukula, K. Lin, Y. Lu, J. Shen, D. Z. Chang, D. Li, G. L. Johanning, F. Wang-Johanning, Downregulation of human endogenous retrovirus type K (HERV-K) Viral env RNA in pancreatic cancer cells decreases cell proliferation and tumor growth. *Clin. Cancer Res.* **23**, 5892–5911 (2017).
27. E.-J. Ko, M.-S. Ock, Y.-H. Choi, J. L. Iovanna, S. Mun, K. Han, H.-S. Kim, H.-J. Cha, Human endogenous retrovirus (HERV)-K env gene knockout affects tumorigenic characteristics of nupr1 gene in DLD-1 colorectal cancer cells. *Int. J. Mol. Sci.* **22**, 3941 (2021).
28. Y. Masuda, R. Ishihara, Y. Murakami, S. Watanabe, Y. Asao, N. Gotoh, T. Kasamatsu, H. Takei, N. Kobayashi, T. Saitoh, H. Murakami, H. Handa, Clinical significance of human endogenous retrovirus K (HERV-K) in multiple myeloma progression. *Int. J. Hematol.* **117**, 563–577 (2023).
29. J. Zhao, K. Rycaj, S. Geng, M. Li, J. B. Plummer, B. Yin, H. Liu, X. Xu, Y. Zhang, Y. Yan, S. A. Glynn, T. H. Dorsey, S. Ambs, G. L. Johanning, L. Gu, F. Wang-Johanning, Expression of human endogenous retrovirus type K envelope protein is a novel candidate prognostic marker for human breast cancer. *Genes Cancer* **2**, 914 (2011).
30. F. Reynier, T. Verjat, F. Turrel, P. E. Imbert, H. Marotte, B. Mougin, P. Miossec, Increase in human endogenous retrovirus HERV-K (HML-2) viral load in active rheumatoid arthritis. *Scand. J. Immunol.* **70**, 295–299 (2009).
31. J. Sicat, N. Sutkowski, B. T. Huber, Expression of human endogenous retrovirus HERV-K18 superantigen is elevated in juvenile rheumatoid arthritis. *J. Rheumatol.* **32**, 1821–1831 (2005).
32. A. Laine, X. Wang, K. Ni, S. E. B. Smith, R. Najjar, L. S. Whitmore, M. Yacoub, A. Bays, M. Gale, T. Mustelin, Expression of envelope protein encoded by endogenous retrovirus K102 in rheumatoid arthritis neutrophils. *Microorganisms* **11**, 1310 (2023).
33. A. I. Khadjinova, X. Wang, A. Laine, K. Ukadike, M. Eckert, A. Stevens, A. A. Bengtsson, C. Lood, T. Mustelin, Autoantibodies against the envelope proteins of endogenous retroviruses K102 and K108 in patients with systemic lupus erythematosus correlate with active disease. *Clin. Exp. Rheumatol.* **40**, 1306–1312 (2022).
34. P. W. Halcrow, D. N. K. Quansah, N. Kumar, J. P. Steiner, A. Nath, J. D. Geiger, HERV-K (HML-2) envelope protein induces mitochondrial depolarization and neurotoxicity via endolysosome iron dyshomeostasis. *J. Neurosci.* **44**, e0826232024 (2024).
35. J. P. Steiner, M. Bachani, N. Malik, C. DeMarino, W. Li, K. Sampson, M.-H. Lee, J. Kowalak, M. Bhaskar, T. Doucet-O'Hare, M. Garcia-Montojo, M. Cowen, B. Smith, L. B. Reoma, J. Medina, J. Brunel, J. Pierquin, B. Charvet, H. Perron, A. Nath, Human endogenous retrovirus K envelope in spinal fluid of amyotrophic lateral sclerosis is toxic. *Ann. Neurol.* **92**, 545–561 (2022).
36. G. Mameli, G. L. Erre, E. Caggiu, S. Mura, D. Cossu, M. Bo, M. L. Cadoni, A. Piras, N. Mundula, E. Colombo, G. Buscetta, G. Passiu, L. A. Sechi, Identification of a HERV-K env surface peptide highly recognized in rheumatoid arthritis (RA) patients: A cross-sectional case–control study. *Clin. Exp. Immunol.* **189**, 127–131 (2017).
37. X. Wang, A. Hefton, K. Ni, K. C. Ukadike, M. A. Bowen, M. Eckert, A. Stevens, C. Lood, T. Mustelin, Autoantibodies against unmodified and citrullinated human endogenous retrovirus K envelope protein in patients with rheumatoid arthritis. *J. Rheumatol.* **49**, 26–35 (2022).
38. M. Noli, G. Meloni, S. Ruberto, S. Jasemi, E. R. Simula, D. Cossu, M. Bo, M. Palermo, L. A. Sechi, HERV-K envelope protein induces long-lasting production of autoantibodies in T1DM patients at onset in comparison to ZNT8 autoantibodies. *Pathogens* **11**, 1188 (2022).
39. K. W. Ng, J. Boumelha, K. S. S. Enfield, J. Almagro, H. Cha, O. Pich, T. Karasaki, D. A. Moore, R. Salgado, M. Sivakumar, G. Young, M. Molina-Arcas, S. de Carné Trécesson, P. Anastasiou, A. Fendler, L. Au, S. T. C. Shepherd, C. Martínez-Ruiz, C. Puttick, J. R. M. Black, T. B. K. Watkins, H. Kim, S. Shim, N. Faulkner, J. Attig, S. Veeriah, N. Magno, S. Ward, A. M. Frankell, M. A. Bakir, E. L. Lim, M. S. Hill, G. A. Wilson, D. E. Cook, N. J. Birkbak, A. Behrens, N. Yousaf, S. Popat, A. Hackshaw, TRACERx Consortium, CAPTURE Consortium, C. T. Hiley, K. Litchfield, N. M. Granahan, M. Jamal-Hanjani, J. Larkin, S.-H. Lee, S. Turajlic, C. Swanton, J. Downward, G. Kassiotis, Antibodies against endogenous retroviruses promote lung cancer immunotherapy. *Nature* **124**, 563–573 (2023).
40. F. Wang-Johanning, K. Rycaj, J. B. Plummer, M. Li, B. Yin, K. Frerich, J. G. Garza, J. Shen, K. Lin, P. Yan, S. A. Glynn, T. H. Dorsey, K. K. Hunt, S. Ambs, G. L. Johanning, Immunotherapeutic potential of anti-human endogenous retrovirus-K envelope protein antibodies in targeting breast tumors. *J. Natl. Cancer Inst.* **104**, 189–210 (2012).
41. J. Krishnamurthy, B. A. Rabinovich, T. Mi, K. C. Switzer, S. Olivares, S. N. Maiti, J. B. Plummer, H. Singh, P. R. Kumaresan, H. M. Huls, F. Wang-Johanning, L. J. N. Cooper, Genetic engineering of T cells to target HERV-K, an ancient retrovirus on melanoma. *Clin. Cancer Res.* **21**, 3241–3251 (2015).
42. F. Zhou, J. Krishnamurthy, Y. Wei, M. Li, K. Hunt, G. L. Johanning, L. J. N. Cooper, F. Wang-Johanning, Chimeric antigen receptor T cells targeting HERV-K inhibit breast cancer and its metastasis through downregulation of Ras. *Oncoimmunology* **4**, e1047582 (2015).
43. B. Kraus, K. Fischer, S. M. Büchner, W. S. Wels, R. Löwer, K. Sliva, B. S. Schnierle, Vaccination directed against the human endogenous retrovirus-K envelope protein inhibits tumor growth in a murine model system. *PLOS ONE* **8**, e72756 (2013).
44. A. Ruggieri, E. Maldener, M. Sauter, N. Mueller-Lantzsch, E. Meese, O. T. Fackler, J. Mayer, Human endogenous retrovirus HERV-K(HML-2) encodes a stable signal peptide with biological properties distinct from Rec. *Retrovirology* **6**, 17 (2009).
45. M. Dewannieux, F. Harper, A. Richaud, C. Letzelter, D. Ribet, G. Pierron, T. Heidmann, Identification of an infectious progenitor for the multiple-copy HERV-K human endogenous retroelements. *Genome Res.* **16**, 1548–1556 (2006).
46. Y. N. Lee, P. D. Bieniasz, Reconstitution of an infectious human endogenous retrovirus. *PLOS Pathog.* **3**, e10 (2007).
47. P. Kramer, V. Lausch, A. Volkwein, K. Hanke, O. Hohn, N. Bannert, The human endogenous retrovirus K(HML-2) has a broad envelope-mediated cellular tropism and is prone to inhibition at a post-entry, pre-integration step. *Virology* **487**, 121–128 (2016).
48. J. E. Henzy, J. M. Coffin, Betaretroviral envelope subunits are noncovalently associated and restricted to the mammalian class. *J. Virol.* **87**, 1937–1946 (2013).
49. P. M. Colman, M. C. Lawrence, The structural biology of type I viral membrane fusion. *Nat. Rev. Mol. Cell Biol.* **4**, 309–319 (2003).
50. J. M. White, S. E. Delos, M. Brecher, K. Schornberg, Structures and mechanisms of viral membrane fusion proteins: Multiple variations on a common theme. *Crit. Rev. Biochem. Mol. Biol.* **43**, 189–219 (2008).
51. H. Ebel, T. Benecke, B. Vollmer, Stabilisation of viral membrane fusion proteins in prefusion conformation by structure-based design for structure determination and vaccine development. *Viruses* **14**, 1816 (2022).

52. X. Yang, L. Florin, M. Farzan, P. Kolchinsky, P. D. Kwong, J. Sodroski, R. Wyatt, Modifications that stabilize human immunodeficiency virus envelope glycoprotein trimers in solution. *J. Virol.* **74**, 4746–4754 (2000).
53. B. Pedenko, G. Sulbaran, D. Guilligay, G. Effantin, W. Weissenhorn, SARS-CoV-2 S glycoprotein stabilization strategies. *Viruses* **15**, 558 (2023).
54. J. Jumper, R. Evans, A. Pritzel, T. Green, M. Figurnov, O. Ronneberger, K. Tunyasuvunakool, R. Bates, A. Žídek, A. Potapenko, A. Bridgland, C. Meyer, S. A. A. Kohl, A. J. Ballard, A. Cowie, B. Romera-Paredes, S. Nikolov, R. Jain, J. Adler, T. Back, S. Petersen, D. Reiman, E. Clancy, M. Zielinski, M. Steinegger, M. Pacholska, T. Berghammer, S. Bodenstein, D. Silver, O. Vinyals, A. W. Senior, K. Kavukcuoglu, P. Kohli, D. Hassabis, Highly accurate protein structure prediction with AlphaFold. *Nature* **596**, 583–589 (2021).
55. J. Ludwiczak, A. Winski, K. Szczepaniak, V. Alva, S. Dunin-Horkawicz, DeepCoil-a fast and accurate prediction of coiled-coil domains in protein sequences. *Bioinformatics* **35**, 2790–2795 (2019).
56. E. F. Pettersen, T. D. Goddard, C. C. Huang, E. C. Meng, G. S. Couch, T. I. Croll, J. H. Morris, T. E. Ferrin, UCSF ChimeraX: Structure visualization for researchers, educators, and developers. *Protein Sci.* **30**, 70–82 (2021).
57. D. B. Craig, A. A. Dombkowski, Disulfide by Design 2.0: A web-based tool for disulfide engineering in proteins. *BMC Bioinformatics* **14**, 346 (2013).
58. L. R. Robinson, S. P. J. Whelan, Infectious entry pathway mediated by the human endogenous retrovirus K envelope protein. *J. Virol.* **90**, 3640–3649 (2016).
59. A. Punjani, J. L. Rubinstein, D. J. Fleet, M. A. Brubaker, cryoSPARC: Algorithms for rapid unsupervised cryo-EM structure determination. *Nat. Methods* **14**, 290–296 (2017).
60. D. Lyumkis, J.-P. Julien, N. de Val, A. Cupo, C. S. Potter, P.-J. Klasse, D. R. Burton, R. W. Sanders, J. P. Moore, B. Carragher, I. A. Wilson, A. B. Ward, Cryo-EM structure of a fully glycosylated soluble cleaved HIV-1 envelope trimer. *Science* **342**, 1484–1490 (2013).
61. J. E. Lee, M. L. Fusco, A. J. Hessell, W. B. Oswald, D. R. Burton, E. O. Saphire, Structure of the Ebola virus glycoprotein bound to an antibody from a human survivor. *Nature* **454**, 177–182 (2008).
62. J. S. McLellan, M. Chen, S. Leung, K. W. Graepel, X. Du, Y. Yang, T. Zhou, U. Baxa, E. Yasuda, T. Beaumont, A. Kumar, K. Modjarrad, Z. Zheng, M. Zhao, N. Xia, P. D. Kwong, B. S. Graham, Structure of RSV fusion glycoprotein trimer bound to a prefusion-specific neutralizing antibody. *Science* **340**, 1113–1117 (2013).
63. I. A. Wilson, J. J. Skehel, D. C. Wiley, Structure of the haemagglutinin membrane glycoprotein of influenza virus at 3 A resolution. *Nature* **289**, 366–373 (1981).
64. D. Wrapp, Z. Mu, B. Thakur, K. Janowska, O. Ajayi, M. Barr, R. Parks, K. Mansouri, R. J. Edwards, B. H. Hahn, P. Acharya, K. O. Saunders, B. F. Haynes, Structure-based stabilization of SOSIP env enhances recombinant ectodomain durability and yield. *J. Virol.* **97**, e0167322 (2023).
65. Y.-X. Tsai, N.-E. Chang, K. Reuter, H.-T. Chang, T.-J. Yang, S. von Bülow, V. Sehrawat, N. Zerrouki, M. Tuffery, M. Gecht, I. L. Grothaus, L. Colombi Ciacchi, Y.-S. Wang, M.-F. Hsu, K.-H. Khoo, G. Hummer, S.-T. D. Hsu, C. Hanus, M. Sikora, Rapid simulation of glycoprotein structures by grafting and steric exclusion of glycan conformer libraries. *Cell* **187**, 1296–1311.e26 (2024).
66. M. Gholami Barzoki, S. Shatizadeh Malekshahi, Z. Heydarifard, M. J. Mahmodi, H. Soltanghoraee, The important biological roles of Syncytin-1 of human endogenous retrovirus W (HERV-W) and Syncytin-2 of HERV-FRD in the human placenta development. *Mol. Biol. Rep.* **50**, 7901–7907 (2023).
67. P. Priščáková, M. Svoboda, Z. Feketová, J. Hutník, V. Repiská, H. Gbelcová, L. Gergely, Syncytin-1, syncytin-2 and suppressyn in human health and disease. *J. Mol. Med. (Berl)* **101**, 1527–1542 (2023).
68. A. Dupressoir, C. Lavialle, T. Heidmann, From ancestral infectious retroviruses to bona fide cellular genes: Role of the captured syncytins in placentation. *Placenta* **33**, 663–671 (2012).
69. M. Merchant, C. P. Mata, Y. Liu, H. Zhai, A. V. Protasio, Y. Modis, A bioactive phlebovirus-like envelope protein in a hookworm endogenous virus. *Sci. Adv.* **8**, eabj6894 (2022).
70. R. Andrabi, J. Pallesen, J. D. Allen, G. Song, J. Zhang, N. de Val, G. Gegg, K. Porter, C.-Y. Su, M. Pauthner, A. Newman, H. Bouton-Verville, F. Garces, I. A. Wilson, M. Crispin, B. H. Hahn, B. F. Haynes, L. Verkoczy, A. B. Ward, D. R. Burton, The chimpanzee SIV envelope trimer: Structure and deployment as an HIV vaccine template. *Cell Rep.* **27**, 2426–2441.e6 (2019).
71. H. T. Nguyen, Q. Wang, S. Anang, J. G. Sodroski, Characterization of the human immunodeficiency virus (HIV-1) envelope glycoprotein conformational states on infectious virus particles. *J. Virol.* **97**, e0185722 (2023).
72. M. van Kempen, S. S. Kim, C. Tumescheit, M. Mirdita, J. Lee, C. L. M. Gilchrist, J. Söding, M. Steinegger, Fast and accurate protein structure search with Foldseek. *Nat. Biotechnol.* **42**, 243–246 (2024).
73. L. Holm, Dali server: Structural unification of protein families. *Nucleic Acids Res.* **50**, W210–W215 (2022).
74. J. Söding, A. Biegert, A. N. Lupas, The HHpred interactive server for protein homology detection and structure prediction. *Nucleic Acids Res.* **33**, W244–W248 (2005).
75. A. Vargas, J. Moreau, S. Landry, F. LeBellego, C. Toufaily, E. Rassart, J. Lafond, B. Barbeau, Syncytin-2 plays an important role in the fusion of human trophoblast cells. *J. Mol. Biol.* **392**, 301–318 (2009).
76. M. Martinez-Molledo, E. Nji, N. Reyes, Structural insights into the lysophospholipid brain uptake mechanism and its inhibition by syncytin-2. *Nat. Struct. Mol. Biol.* **29**, 604–612 (2022).
77. C. D. Higgins, V. N. Malashkevich, S. C. Almo, J. R. Lai, Influence of a heptad repeat stutter on the pH-dependent conformational behavior of the central coiled-coil from influenza hemagglutinin HA2: The heptad repeat stutter in influenza HA2. *Proteins* **82**, 2220–2228 (2014).
78. W. Weissenhorn, A. Carfí, K. H. Lee, J. J. Skehel, D. C. Wiley, Crystal structure of the Ebola virus membrane fusion subunit, GP2, from the envelope glycoprotein ectodomain. *Mol. Cell* **2**, 605–616 (1998).
79. S. Igonet, M.-C. Vaney, C. Vonrhein, G. Bricogne, E. A. Stura, H. Hengartner, B. Eschli, F. A. Rey, X-ray structure of the arenavirus glycoprotein GP2 in its postfusion hairpin conformation. *Proc. Natl. Acad. Sci. U.S.A.* **108**, 19967–19972 (2011).
80. K. Ruigrok, M.-C. Vaney, J. Buchrieser, E. Baquero, J. Hellert, B. Baron, P. England, O. Schwartz, F. A. Rey, M. Backovic, X-ray structures of the post-fusion 6-helix bundle of the human syncytins and their functional implications. *J. Mol. Biol.* **431**, 4922–4940 (2019).
81. J. H. Brown, C. Cohen, D. A. Parry, Heptad breaks in α-helical coiled coils: Stutters and stammers. *Proteins* **26**, 134–145 (1996).
82. M. S. Ladinsky, P. N. Gnanapragasam, Z. Yang, A. P. West, M. S. Kay, P. J. Bjorkman, Electron tomography visualization of HIV-1 fusion with target cells using fusion inhibitors to trap the pre-hairpin intermediate. *eLife* **9**, e58411 (2020).
83. C. Riedel, D. Vasishtan, C. A. Siebert, C. Whittle, M. J. Lehmann, W. Mothes, K. Grünewald, Native structure of a retroviral envelope protein and its conformational change upon interaction with the target cell. *J. Struct. Biol.* **197**, 172–180 (2017).
84. A. Serafino, E. Balestrieri, P. Pierimarchi, C. Matteucci, G. Moroni, E. Oricchio, G. Rasi, A. Mastino, C. Spadafora, E. Garaci, P. S. Vallebona, The activation of human endogenous retrovirus K (HERV-K) is implicated in melanoma cell malignant transformation. *Exp. Cell Res.* **315**, 849–862 (2009).
85. E. Stricker, E. C. Peckham-Gregory, M. E. Scheurer, HERVs and cancer—A comprehensive review of the relationship of human endogenous retroviruses and human cancers. *Biomedicine* **11**, 936 (2023).
86. S. Levet, J. Medina, J. Joanou, A. Demolder, N. Queruel, K. Réant, M. Normand, M. Seffals, J. Dimier, R. Germi, T. Piofczyk, J. Portoukalian, J. L. Touraine, H. Perron, An ancestral retroviral protein identified as a therapeutic target in type-1 diabetes. *JCI Insight* **2**, e94387 (2017).
87. V. Gröger, H. Cynis, Human endogenous retroviruses and their putative role in the development of autoimmune disorders such as multiple sclerosis. *Front. Microbiol.* **9**, 265 (2018).
88. G. L. Adler, K. Le, Y. Fu, W. S. Kim, Human endogenous retroviruses in neurodegenerative diseases. *Genes (Basel)* **15**, 745 (2024).
89. T. Wang, M. Medynets, K. R. Johnson, T. T. Doucet-O'Hare, B. DiSanza, W. Li, Y. Xu, A. Bagnell, R. Tyagi, K. Sampson, N. Malik, J. Steiner, A. Hadegan, J. Kowalak, J. O'Malley, D. Maric, A. Nath, Regulation of stem cell function and neuronal differentiation by HERV-K via mTOR pathway. *Proc. Natl. Acad. Sci. U.S.A.* **117**, 17842–17853 (2020).
90. Z. Zou, T. Tao, H. Li, X. Zhu, mTOR signaling pathway and mTOR inhibitors in cancer: Progress and challenges. *Cell Biosci.* **10**, 31 (2020).
91. M. Dewannieux, S. Blaise, T. Heidmann, Identification of a functional envelope protein from the HERV-K family of human endogenous retroviruses. *J. Virol.* **79**, 15573–15577 (2005).
92. A. Kleiman, N. Senyuta, A. Tryakin, M. Sauter, A. Karseladze, S. Tjulandin, V. Gurtsevitch, N. Mueller-Lantzsch, HERV-K(HML-2) GAG/ENV antibodies as indicator for therapy effect in patients with germ cell tumors. *Int. J. Cancer* **110**, 459–461 (2004).
93. C. A. Hervé, E. B. Lugli, A. Brand, D. J. Griffiths, P. J. W. Venables, Autoantibodies to human endogenous retrovirus-K are frequently detected in health and disease and react with multiple epitopes. *Clin. Exp. Immunol.* **128**, 75–82 (2002).
94. R. Shaked, M. Katz, H. Cohen-Dvashi, R. Diskin, The prefusion structure of the HERV-K (HML-2) Env spike complex. bioRxiv 644160 [Preprint] (2025). https://doi.org/10.1101/2025.03.19.644160.
95. V. Estrella, T. Chen, M. Lloyd, J. Wojtkowiak, H. H. Cornnell, A. Ibrahim-Hashim, K. Bailey, Y. Balagurunathan, J. M. Rothberg, B. F. Sloane, J. Johnson, R. A. Gatenby, R. J. Gillies, Acidity generated by the tumor microenvironment drives local invasion. *Cancer Res.* **73**, 1524–1535 (2013).
96. E. Boedtkjer, S. F. Pedersen, The acidic tumor microenvironment as a driver of cancer. *Annu. Rev. Physiol.* **82**, 103–126 (2020).
97. L. R. Robinson-McCarthy, K. R. McCarthy, M. Raaben, S. Piccinotti, J. Nieuwenhuis, S. H. Stubbs, M. J. G. Bakkers, S. P. J. Whelan, Reconstruction of the cell entry pathway of an extinct virus. *PLoS Pathog.* **14**, e1007123 (2018).
98. S. Hosseiniporgham, L. A. Sechi, Anti-HERV-K drugs and vaccines, possible therapies against tumors. *Vaccines (Basel)* **11**, 751 (2023).
99. F. Spriano, L. Cascione, J. Sgrignani, N. Bendik, S. Napoli, G. Sartori, E. Cannas, T. Gong, A. J. Arribas, M. Pizzi, D. Rossi, D. F. Robbiani, A. Cavalli, F. Bertoni, Characterization of a

novel humanized heavy chain antibody targeting endogenous retroviruses with anti-lymphoma activity. bioRxiv 576027 [Preprint] (2024). https://doi.org/10.1101/2024.01.17.576027.
100. M. Silva, Y. Kato, M. B. Melo, I. Phung, B. L. Freeman, Z. Li, K. Roh, J. W. Van Wijnbergen, H. Watkins, C. A. Enemuo, B. L. Hartwell, J. Y. H. Chang, S. Xiao, K. A. Rodrigues, K. M. Cirelli, N. Li, S. Haupt, A. Aung, B. Cossette, W. Abraham, S. Kataria, R. Bastidas, J. Bhiman, C. Linde, N. I. Bloom, B. Groschel, E. Georgeson, N. Phelps, A. Thomas, J. Bals, D. G. Carnathan, D. Lingwood, D. R. Burton, G. Alter, T. P. Padera, A. M. Belcher, W. R. Schief, G. Silvestri, R. M. Ruprecht, S. Crotty, D. J. Irvine, A particulate saponin/TLR agonist vaccine adjuvant alters lymph flow and modulates adaptive immunity. *Sci. Immunol.* **6**, eabf1152 (2021).
101. T. G. Martin, A. Boland, A. W. P. Fitzpatrick, S. H. W. Scheres, Graphene oxide grid preparation (2016); https://doi.org/10.6084/m9.figshare.3178669.v1.
102. K. Jamali, L. Käll, R. Zhang, A. Brown, D. Kimanius, S. H. W. Scheres, Automated model building and protein identification in cryo-EM maps. *Nature* **628**, 450–457 (2024).
103. P. Emsley, B. Lohkamp, W. G. Scott, K. Cowtan, Features and development of Coot. *Acta Crystallogr. D Biol. Crystallogr.* **66**, 486–501 (2010).
104. P. Emsley, K. Cowtan, Coot: Model-building tools for molecular graphics. *Acta Crystallogr. D Biol. Crystallogr.* **60**, 2126–2132 (2004).
105. J. Abramson, J. Adler, J. Dunger, R. Evans, T. Green, A. Pritzel, O. Ronneberger, L. Willmore, A. J. Ballard, J. Bambrick, S. W. Bodenstein, D. A. Evans, C.-C. Hung, M. O'Neill, D. Reiman, K. Tunyasuvunakool, Z. Wu, A. Žemgulytė, E. Arvaniti, C. Beattie, O. Bertolli, A. Bridgland, A. Cherepanov, M. Congreve, A. I. Cowen-Rivers, A. Cowie, M. Figurnov, F. B. Fuchs, H. Gladman, R. Jain, Y. A. Khan, C. M. R. Low, K. Perlin, A. Potapenko, P. Savy, S. Singh, A. Stecula, A. Thillaisundaram, C. Tong, S. Yakneen, E. D. Zhong, M. Zielinski, A. Žídek, V. Bapst, P. Kohli, M. Jaderberg, D. Hassabis, J. M. Jumper, Accurate structure prediction of biomolecular interactions with AlphaFold 3. *Nature* **630**, 493–500 (2024).
106. R. Sanchez-Garcia, J. Gomez-Blanco, A. Cuervo, J. M. Carazo, C. O. S. Sorzano, J. Vargas, DeepEMhancer: A deep learning solution for cryo-EM volume post-processing. *Commun. Biol.* **4**, 874 (2021).
107. D. Liebschner, P. V. Afonine, M. L. Baker, G. Bunkóczi, V. B. Chen, T. I. Croll, B. Hintze, L. W. Hung, S. Jain, A. J. McCoy, N. W. Moriarty, R. D. Oeffner, B. K. Poon, M. G. Prisant, R. J. Read, J. S. Richardson, D. C. Richardson, M. D. Sammito, O. V. Sobolev, D. H. Stockwell, T. C. Terwilliger, A. G. Urzhumtsev, L. L. Videau, C. J. Williams, P. D. Adams, Macromolecular structure determination using x-rays, neutrons and electrons: Recent developments in Phenix. *Acta Crystallogr. D Struct. Biol.* **75**, 861–877 (2019).
108. C. J. Williams, J. J. Headd, N. W. Moriarty, M. G. Prisant, L. L. Videau, L. N. Deis, V. Verma, D. A. Keedy, B. J. Hintze, V. B. Chen, S. Jain, S. M. Lewis, W. B. Arendall III, J. Snoeyink, P. D. Adams, S. C. Lovell, J. S. Richardson, D. C. Richardson, MolProbity: More and better reference data for improved all-atom structure validation. *Protein Sci.* **27**, 293–315 (2018).
109. UniProt Consortium, UniProt: The universal protein knowledgebase in 2023. *Nucleic Acids Res.* **51**, D523–D531 (2023).
110. F. Sievers, A. Wilm, D. Dineen, T. J. Gibson, K. Karplus, W. Li, R. Lopez, H. McWilliam, M. Remmert, J. Söding, J. D. Thompson, D. G. Higgins, Fast, scalable generation of high-quality protein multiple sequence alignments using Clustal Omega. *Mol. Syst. Biol.* **7**, 539 (2011).
111. P. V. Troshin, J. B. Procter, G. J. Barton, Java bioinformatics analysis web services for multiple sequence alignment—JABAWS:MSA. *Bioinformatics* **27**, 2001–2002 (2011).
112. R. Gupta, S. Brunak, Prediction of glycosylation across the human proteome and the correlation to protein function. *Pac. Symp. Biocomput.*, 310–322 (2002).

Acknowledgments: We would like to thank S. Schendel for reviewing and editing the manuscript. We acknowledge the cryo-EM facility of La Jolla Institute for Immunology for assistance in grid preparation and data collection, and equipment supported by the GHR Foundation and other generous private donors. **Funding:** This research was supported by a Curebound discovery grant (13502-01-000-408) to E.O.S., by LJI & Kyowa Kirin Inc. [KKNA Kyowa Kirin North America to E.O.S., and by a Kyowa Kirin North America accelerator grant (18030-01-000-408) to J.S.]. **Author contributions:** Conceptualization: J.S., C.S., K.M.H., V.I.L, T.M., and E.O.S. Data curation: J.S., C.S., E.M.W., D.S.Z., K.M.H., R.D.A., and T.M. Formal analysis: J.S., C.S., E.M.W., C.H., and E.O.S. Funding acquisition: J.S., V.I.L., T.M., and E.O.S. Investigation: J.S., C.S., E.M.W., F.M., R.R.R., P.J.P., S.S.H., D.P., C.H., C.Y., K.C.L.S., V.I.L., R.D.A., and T.M. Methodology: J.S., C.S., R.R.R., K.M.H., D.S.Z., T.M., and E.O.S. Project administration: J.S., T.M., and E.O.S. Resources: J.S., T.M., and E.O.S. Supervision: J.S., K.M.H., T.M., and E.O.S. Validation: J.S., C.S., E.M.W., P.J.P., D.S.Z., and T.M. Visualization: J.S., C.S., and T.M. Writing—original draft: J.S., C.S., and F.M. Writing—review and editing: J.S., C.S., F.M., K.M.H., D.S.Z., T.M., and E.O.S. **Competing interests:** The La Jolla Institute for Immunology has pending provisional patent coverage on the mAbs and proteins described herein. The applications, entitled "HERV-K Envelope Protein Binders and Compositions and Methods of Use Thereof" and "Stabilized Pre-Fusion HERV-K Envelope Ectodomain Trimer" lists inventors E.O.S., K.M.H., S.H., E.M.W., and J.S., respectively, and were assigned US Provisional Patent nos. 63/638,067 and 63/783,708. The authors declare that they have no other competing interests. **Data and materials availability:** The apo prefusion-stabilized HERV-K Env_{ECTO}, Kenv-6 bound prefusion HERV-K Env_{ECTO}, and Kenv-4 bound postfusion TM_{ECTO} cryo-EM maps have been deposited to the EM Database with codes EMD-70098, EMD-48351, and EMD-48374, respectively. Atomic models are deposited in the Protein Data Bank with accession codes 9O4F, 9MLA, and 9MLK. The mAbs and proteins presented in this study can be provided by the La Jolla Institute for Immunology pending scientific review and a completed material transfer agreement. Requests for the reagents should be submitted to E.O.S. at erica@lji.org.

Submitted 7 May 2025
Accepted 25 July 2025
Published 27 August 2025
10.1126/sciadv.ady8168